Joint Graduate School of Veterinary Medicine,

Kagoshima University

Molecular biological studies on host cell responses involving rabies virus matrix protein

狂犬病ウイルス M 蛋白質が関与する宿主細胞応答の分子生物学的研究

A thesis submitted to The Joint Graduate School of Veterinary Medicine, Kagoshima University for the degree of Doctor of Philosophy (Ph.D.)

By

Isshu Kojima

November 2022

Contents

Preface 1-7

Chapter I 8-20

Identification of viral protein and responsible amino acid involved in stress granule formation in cells infected with rabies virus

Introduction 9

Materials and methods 10-12

Results 13-15

Discussion 16-17

Figures 18-20

Chapter II 21-47

Mechanism of stress granule formation related to the amino acid at position 95 in rabies virus matrix protein

Introduction 22-23

Materials and methods 24-31

Results 32-36

Discussion 37-40

Figures 41-47

Chapter III 48-76

Involvement of programmed cell death related to the amino acid at position 95 in rabies virus matrix protein

Introduction 49-50

Materials and methods 51-55

Results 56-60

Discussion 61-67

Figures 68-76

Concluding Remarks 77-78

Acknowledgment 79-82

References 83-99

Preface

Rabies is a fatal viral zoonosis characterized by neurological symptoms. The causative agent, the rabies virus (RABV), infects almost all mammals, including humans. Currently, there is no effective cure for this disease, leading to a high fatality rate of up to 100%. Rabies occurs almost worldwide except in Japan, the United Kingdom, Oceania, and Northern Europe. Dogs are the primary reservoir in Asia and Africa, whereas wild animals such as foxes and skunks are the primary reservoirs in Europe and North America. Even at present, approximately 59,000 deaths are reported annually worldwide, especially in developing countries (1), and thus, countermeasures are urgently needed.

Fortunately, rabies can be prevented by vaccination (2). Furthermore, even after being bitten by an infected animal, the development of the disease can be prevented by vaccinating the patient before the onset of the disease. Rabies vaccines are of two types: inactivated and live vaccines. Inactivated vaccines are produced by growing attenuated viruses in cultured cells, followed by their inactivation and purification with a chemical agent (2). Inactivated vaccines are widely used in humans and dogs worldwide because there is no risk of virulence reversion. However, inactivated vaccines are expensive because of their high production costs and are less effective than live vaccines, because

they do not induce cellular immunity and require multiple doses. These disadvantages make it difficult to disseminate inactivated rabies vaccines in developing countries; therefore, they need to be propagated more efficiently to improve productivity. In contrast, live rabies vaccines are exclusively used in wild animals. Live vaccines can be administered orally to animals, such as foxes and stray dogs, by using baits in the field. However, current live vaccines have safety problems because a single mutation in a single amino acid can cause a reversion to virulence.

To date, no effective treatment has been established for post-exposure rabies; in 2004, a case was reported in the U.S. in which an unvaccinated girl survived the onset of rabies by receiving a combination of anesthesia and antiviral drugs (3). The procedure used in this case was called the “Milwaukee Protocol”, and was expected to be a cure for rabies, which had been incurable until then. However, this procedure has been tried in many rabies treatments since then with little success, and even if life could be maintained with this procedure, it often results in coma and other serious sequelae, so it is almost impossible to treat the disease (4). In other words, it is difficult to say that a rabies treatment method has been established. Therefore, it is necessary to accumulate basic information on the mechanisms of viral multiplication and pathogenicity to develop inexpensive and effective vaccines and new treatments for post-disease onset. However,

this information remains largely unknown.

The primary route of RABV transmission is through the bite of a rabid animal. After an incubation period, which typically lasts for weeks or months, RABV spreads through the spinal cord to the brain (5). After entering the brain, RABV replicates extensively, causing central nervous system dysfunction and neurological symptoms, such as paralysis and madness. In general, encephalitis-causing viruses (e.g., herpes simplex virus and Japanese encephalitis virus; JEV) induce severe inflammation in the host brain and programmed cell death, including apoptosis, in infected neurons (6–9). However, degeneration and cell death are rarely observed in the brains of rabid animals and patients; only minor inflammation occurs (10). Therefore, it is believed that RABV evades the host immune response and causes neurological symptoms by functionally disrupting conduction and transmission in neurons without causing cellular damage (11–13). To elucidate the detailed mechanism of RABV pathogenesis, it is necessary to understand the molecular biological effects of viral proteins on host cells.

RABV is a non-segmented negative-sense RNA virus, which is classified as a member of *Lyssavirus* in the family Rhabdoviridae. The RABV genome (~12 kb) encodes five structural proteins: nucleoprotein, phosphoprotein, matrix protein, glycoprotein, and large protein (N, P, M, G, and L proteins, respectively; Fig. i). N, P, and L form the

ribonucleoprotein (RNP) complex that executes viral genome replication and gene transcription (14, 15). M is located on the inner surface of the envelope of the virion and plays an important role in the recruitment and condensation of RNPs to the host cell membrane and in the budding of enveloped viral particles (16, 17). G forms projections on the surface of the viral envelope that bind to host cell receptors (18, 19).

Type I interferons (IFNs) play a central role in innate immune induction during the early stages of viral infection. When viruses infect cells, pattern recognition receptors (PRRs) recognize the infection, resulting in the release of type I IFNs (IFN-α and β) through various signaling pathways (20). Type I IFNs bind to their receptors on the surrounding cells and activate signal transducer and activator of transcription 1 (STAT1), which is a downstream transcription factor that induces the expression of many IFN-stimulated genes (ISGs) and an antiviral state (21, 22). In the case of RABV, retinoic acid-inducible gene I (RIG-I) has been reported to play an important role in the recognition of RABV infection by PRRs (23–25). Furthermore, stress granules (SGs) have been recently reported to regulate RIG-I activation (25–28). SGs are cytoplasmic granules that are transiently formed when cells undergo various stresses, such as chemicals and heat shock, and store untranslated mRNA and RNA-binding proteins (25, 29). Although SGs have been shown to play a role as a “scaffold” where RIG-I senses and activates viral genomics

(30, 31), the relationship between the immune evasion mechanisms by RABV and SGs remains unknown.

Programmed cell death including apoptosis is one of the host biological defenses against viruses (32, 33). Apoptosis is an "active cell death" induced by viral infection or oxidative stress. During viral infection in particular, apoptotic cells activate phagocytes to remove themselves, inhibiting viral spread (32, 34). Interestingly, RABV pathogenesis is negatively correlated with the ability of the virus to induce apoptosis (11, 18). In particular, attenuated RABV strains strongly induce apoptosis in infected cells, whereas highly pathogenic strains are less likely to induce apoptosis (11, 18, 35–37), which explains its non-destructive replication in the brains of rabid animals.

The reverse genetic system, which enables the manipulation of viral genomes, is useful for identifying viral genes that affect host cell responses. RABV strains are broadly categorized into two types: street strains, which are field viruses isolated from naturally infected animals, and fixed strains, which are established by long-term passaging of street strains in animal brain tissue or cultured cells to alter characteristics, such as making incubation periods shorter and constant and reducing peripheral infectivity. To elucidate the innate immune evasion and cell death mechanisms of RABV, reverse genetic analysis of two genetically related fixed virus strains with different virulence has been conducted

(38–40). The Nishigahara strain, a highly pathogenic fixed strain, causes lethal infection in mice after intramuscular and intracerebral inoculation, whereas the Ni-CE strain, an attenuated strain established from 100 passages of the Nishigahara strain in chicken embryo fibroblasts, does not cause any symptoms when inoculated intramuscularly at high doses in mice; even when inoculated intracerebrally, it causes only nonfatal infection with mild symptoms such as transient weight loss (40). However, despite the significant difference in the virulence of the two strains, the homology rate of the whole genome sequences of the two strains is considerably high (99.8%). Therefore, by comparing the characteristics of chimeric viruses in which each gene is swapped between the Nishigahara and Ni-CE strains or point mutant viruses in which amino acids are exchanged between these strains with their respective original strains, it is possible to identify the viral factors that determine differences in host responses at the molecular level.

In this study, at first, I focused on SGs, a scaffold that recognizes viral infections and triggers innate immune response. The SG formation ability of the Nishigahara and Ni-CE strains was analyzed to elucidate the relationship between SG formation and RABV pathogenesis. In chapter I, the amino acid at position 95 in the RABV-M protein (M95) is described to be involved in SG formation. In chapter II, the molecular mechanism of

SG formation related to M95 is elucidated. Chapter III focuses on the previously reported involvement of M95 in cell death (41) and investigates the unknown mechanisms related to M95.

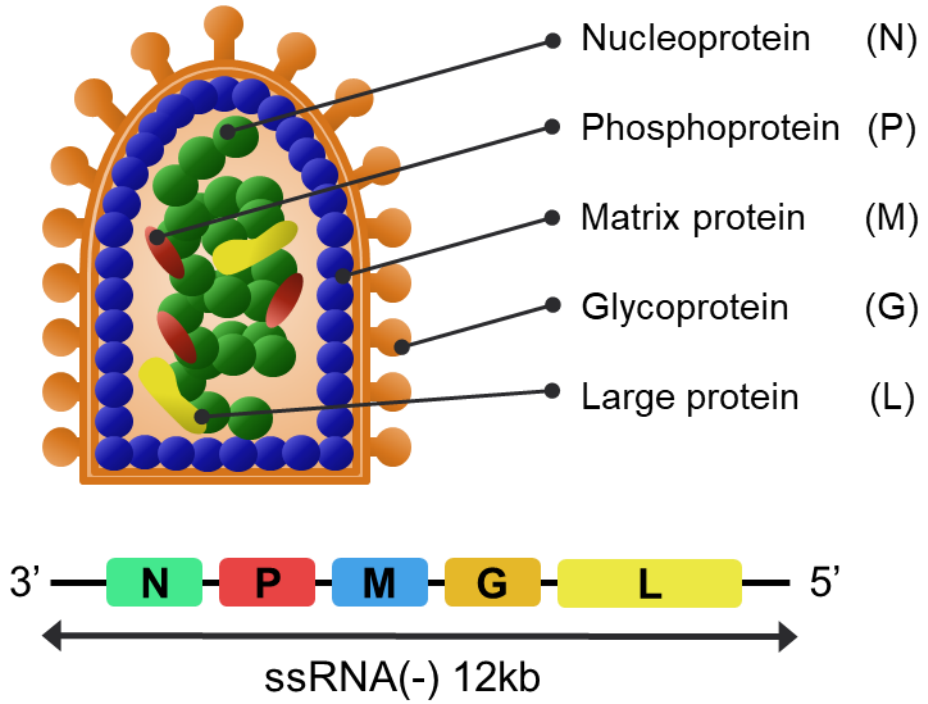

Fig.i. Schematic diagram of structure and genome of rabies virus.

Chapter I

Identification of viral protein and responsible amino acid involved in stress granule formation in cells infected with rabies virus

INTRODUCTION

SGs are non-membranous cytosolic structures formed through a physical process called liquid-liquid phase separation (42, 43). SGs contain small ribosomal subunits, translation initiation factors, as well as translationally arrested mRNA and RNA-binding proteins, such as T cell internal antigen 1 (TIA-1), TIA-1 related protein (TIAR), and RasGAP-associated endoribonuclease 1 (G3BP1) (44, 45). Although their function is still not fully understood, SGs are thought to play an important role in cell regulation. SGs can affect translation by compartmentalizing mRNPs. Moreover, SGs can also influence signaling pathways, such as apoptosis, cell growth, and metabolic control, through the degradation and compartmentalization of cellular proteins and mRNPs (24, 25, 42, 43).

Recently, Nikolic *et al.* reported that fixed RABV strains elicited formation of SGs containing G3BP1 and TIA-1 (46). However, the relation between the antiviral response via SG formation and RABV virulence is not fully understood in the absence of research comparing SG formation between virulent and avirulent strains.

Accordingly, in this chapter, I investigated the difference of SG formation between Nishigahara strain and Ni-CE strain. Furthermore, I attempted to identify viral protein(s) and amino acid(s) with key roles in SG formation by utilizing chimeric viruses and point mutation strains subject to gene substitution.

MATERIALS AND METHODS

Cells

Human embryonic kidney epithelial 293T cells, human neuroblastoma SYM-I cells, and mouse neuroblastoma NA cells were maintained in Eagle's minimum essential medium (E-MEM: Nissui, Tokyo, Japan) adjusted to pH 7.0 with $NaHCO_3$ and supplemented with 10% fetal calf serum (FCS) and 1% penicillin-streptomycin-amphotericin B suspension (FUJIFILM Wako Pure Chemical, Osaka, Japan). These cells were cultured at 37°C in a humidified 5% CO_2 atmosphere.

Viruses

Nishigahara, Ni-CE, chimeric and mutant strains used in this study were recovered from the relevant cloned cDNA as reported previously (40, 41, 47). As street RABV strains, 1088 and Komatsugawa strains were also used (48–50). Stocks of all RABV strains were propagated in NA cells.

Indirect immunofluorescent staining

Cells were cultured on an 8-well chamber slide (SPL Life Sciences, Pocheon, South Korea) and infected with the relevant RABV strain at a multiplicity of infection (MOI) of 1 or 0.03. At 24 hours post-infection (hpi), cells were fixed with 4% paraformaldehyde and then permeabilized for 1 min with methanol (FUJIFILM Wako Pure Chemical). For analyses of SG formation, cells were incubated with anti-RABV N protein mouse monoclonal antibody (1:10,000, mAb; #13-27) (51) and anti-TIA-1 goat antibody (1:500, #sc-1751, Santa Cruz Biotechnology, Dallas, TX, USA), anti-TIAR goat antibody (1:500, #sc-1749, Santa Cruz Biotechnology), or anti-G3BP1 goat antibody (1:500, #sc-70283, Santa Cruz Biotechnology) at 4°C overnight. After washing with phosphate-buffered saline (PBS), secondary antibody solution including Dylight 594 anti-mouse IgG horse antibody (1:2,000, Vector Laboratories, Burlingame, CA, USA), Dylight 488 anti-goat IgG horse antibody (1:2,000,Vector Laboratories), and Hoechst 33342 (1:2,000, DOJINDO Laboratories, Kumamoto, Japan) were added to each well, followed by incubation at 37°C for 1 h. Cells were then mounted using ProLong Diamond Antifade Mountant (Thermo Fisher Scientific, Waltham, MA, USA) and analyzed using an LSM 700 confocal laser scanning microscope (Carl Zeiss, Oberkochen, Germany).

Quantification of SG-forming cells using transient SG-inducible cells

293T cells were cultured in an 8-well chamber slide at 1.0×10^5 cells per well and infected with Nishigahara, Ni-CE, M29-mutanted, or M95-mutated strain at MOI of 1 and fixed at 24hpi. Cells were then fixed and stained for observing SG formation as described above. The numbers of SG-forming and RABV-infected cells were counted with the aid of a confocal laser scanning microscope. More than 300 cells in three random fields were analyzed per sample and the results are expressed as means and standard error (SE).

Statistical analysis

Statistical significance was evaluated using Tukey's test for multiple-group comparisons. Values of $P < 0.05$ were regarded as significant.

RESULTS

SG formation is induced by infection with Ni-CE strain but not infection with Nishigahara and street RABV strains.

To compare the abilities of the Nishigahara and Ni-CE strains to induce SG formation, I investigated the accumulation of SG marker proteins in the cytoplasm of infected cells using an indirect immunofluorescence assay. At 24 hpi, TIA-1, an SG marker protein, showed diffuse staining in the cytoplasm in mock- and Nishigahara-infected 293T cells, whereas TIA-1 showed strong positive staining of cytoplasmic granules in Ni-CE-infected cells (Fig. 1-1A and 1-1B). Notably, almost all granules were localized near cytoplasmic viral factories that stained with RABV N protein-specific antibody, known as Negri bodies (NBs), similar to previous findings (46). The staining of TIAR and G3BP1, also known as SG markers, yielded similar results as those for TIA-1 (Fig. 1-1C and 1-1D). Almost identical results were observed in experiments with SYM-I cells, a human neuroblastoma cell line (data not shown). Furthermore, TIAR showed diffuse staining in the cytoplasm in cells infected with the RABV street strains, 1088 and Komatsugawa (Fig. 1-1E). These results indicate that the avirulent Ni-CE stain, but not

virulent Nishigahara, 1088, and Komatsugawa strains, induce SG formation in infected cells.

The M gene of the Ni-CE strain is the determinant for induction of SG formation.

To determine which RABV protein may be involved in SG formation, 293T cells were infected with Nishigahara, Ni-CE, and chimeric virus strains, including Ni(CEN), Ni(CEP), Ni(CEM), Ni(CEG), and Ni(CEL) (Fig. 1-2A). The chimeric virus strains were created by substituting an Ni-CE strain gene with its equivalent in the Nishigahara genome background (40). The 293T cells infected with the Ni(CEN), Ni(CEP), Ni(CEG), or Ni(CEL) strain did not form SGs, and neither did Nishigahara-infected cells (Fig. 1-2B). On the other hand, cells infected with the Ni(CEM) strain showed SG accumulation in the cytoplasm, as did cells infected with the Ni-CE strain. These results indicate that the M gene plays an important role in promoting SG formation in Ni-CE strain-infected cells.

The amino acid at position 95 in the RABV-M protein plays a critical role in SG formation.

There are two amino acid differences in the M protein at positions 29 and 95 between the Nishigahara and Ni-CE strains (40, 41). Therefore, to determine the M protein amino acid responsible for SG induction, I investigated SG formation in 293T cells infected with Nishigahara, Ni-CE, and mutant strains that had undergone replacement of the amino acid at position 29 (M29) or 95 (M95) in the M protein with Nishigahara or Ni-CE-strain [Ni(CEM29), Ni(CEM95), CE(NiM29), and CE(NiM95)] equivalents (Fig. 1-3A). I found that SGs were more prominent in cells infected with the Ni-CE, Ni(CEM95), or CE(NiM29) strain—where M95 was occupied by alanine (Ala)—than in cells infected with the Nishigahara, Ni(CEM29), or CE(NiM95) strains—where M95 was occupied by valine (Val; Fig. 1-3B). Quantification of SG-forming RABV-infected cells showed that the Ni(CEM95)-infected cells showed higher numbers of SG-forming than Nishigahara-infected cells, while the CE(NiM95)-infected cells showed lower than Ni-CE-infected cells (Fig. 1-3C). Although CE(NiM29)-infected cells showed lower numbers of SG-forming than Ni-CE-infected, CE(NiM29)-infected cells showed higher than cells infected with Nishigahara, Ni(CEM29), or CE(NiM95) strain. These results indicate that the mutation at M95 from Val to Ala is a determinant for SG formation.

DISCUSSION

When cells are infected with viruses, SGs form, suppressing viral replication and inducing antiviral responses (25, 26). Cells infected with RABV also form SGs, but neither the RABV protein responsible for SG formation nor the effects of RABV-induced formation of SGs is fully understood (46). In this chapter, I revealed that the virulent Nishigahara strain does not induce SG formation, whereas the avirulent Ni-CE strain does. I then demonstrated that M95, the known pathogenic determinant of the Nishigahara strain (39), plays a critical role in inhibiting SG formation. To my knowledge, this is the first report showing that amino acids known to determine viral pathogenesis are involved in inhibiting SG formation.

In another report, RABV strains induced SG formation with resultant SGs localized in the vicinity of NBs (46). These SGs co-localized with viral RNA, suggesting they play a role in viral replication. However, my current results show that the Nishigahara strain does not induce SG formation (Fig. 1-1). Furthermore, no SG formation was observed in cells infected with street isolates RABV, 1088 and Komatsugawa, whose amino acids at M95 are preserved at Val (Fig. 1-1E). Considering that the Nishigahara strain, like the Ni-CE strain, was also able to replicate well in tissue culture cells (40), I suggest that SGs

may not be significantly involved in virus replication. However, further investigation is needed, since I did not evaluate SG-viral RNA co-localization in this study.

M95 has been implicated the involvement in pathogenesis and apoptosis. It is previously reported that the Ni-CE strain does not kill mice, but the CE(NiM95) strain does (39). Mita *et al*. investigated the pathogenesis involving M95 and demonstrated that Ni-CE and Ni(CEM95) strains induce cytopathic effect (CPE) drastically, while Nishigahara and CE(NiM95) strains did not i*n vitro*, which is induced by apoptosis (41). In this chapter, I found that M95 did not only play a role in pathogenesis and apoptosis but also in SG formation. The pathogenesis involving M95 may be explained by innate immune evasion arising from the inhibition of the ability to induce SG formation. On the other hand, as mentioned above, the mutation at M95 from Val to Ala also affects the ability to induce cell death (41); this avoidance of cell death inhibits immune system activity and is a characteristic of RABV pathogenesis (11, 52, 53), and thus may also be involved in the pathogenesis of the virus. Further studies are needed to elucidate the mechanism in more detail *in vivo*.

In conclusion, we demonstrated that the high pathogenic Nishigahara strain inhibit SG formation, while the low pathogenic Ni-CE strain did not. Furthermore, I found that M95 is a key determinant for SG formation induced by the Ni-CE strain.

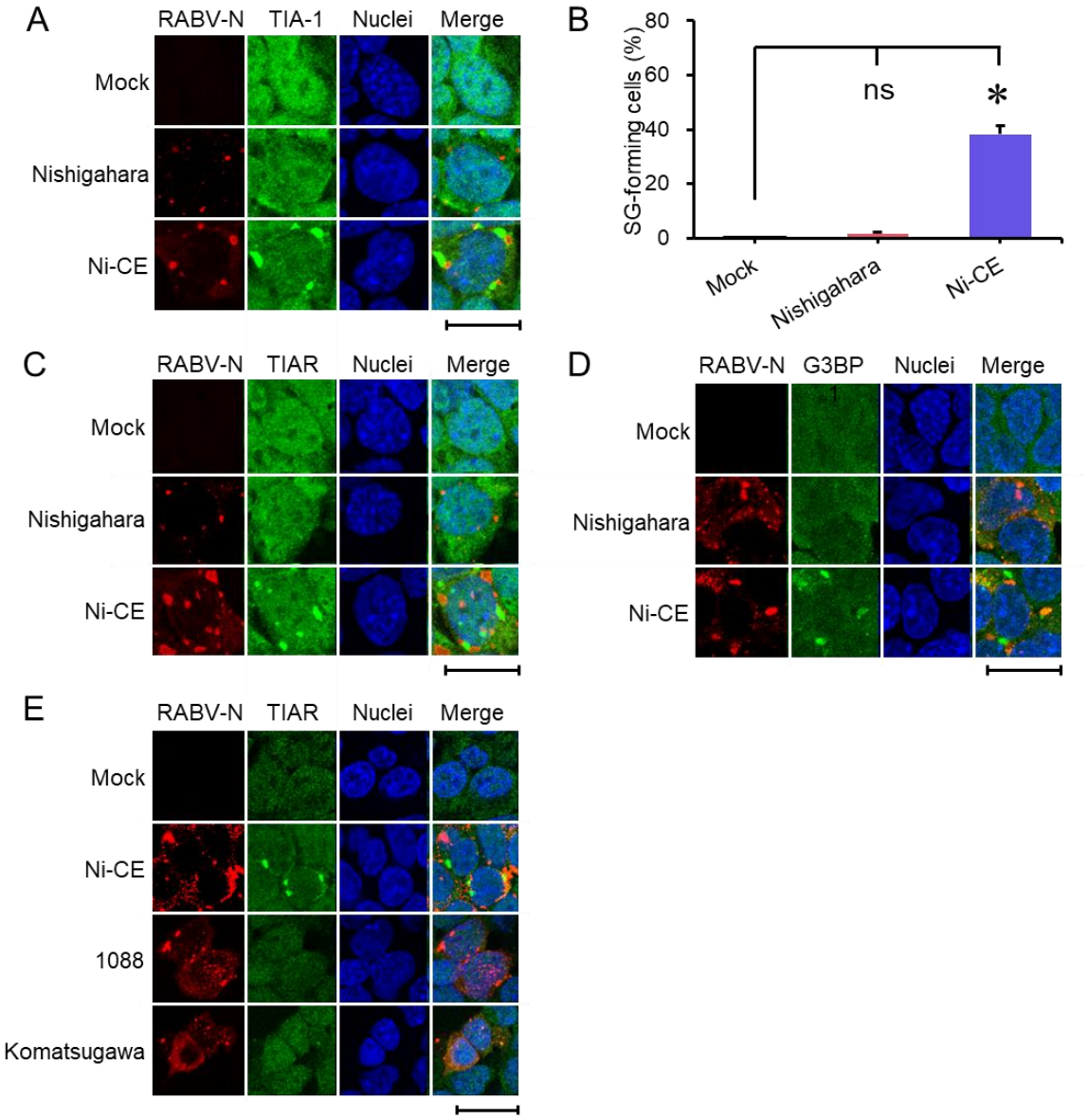

Fig.1-1. Comparison of the SG formation between the Nishigahara, Ni-CE, and field strains. SG marker accumulation in cells infected with the avirulent Ni-CE strain. (A) 293T cells were infected with the relevant strain at an MOI of 1. At 24 hpi, cells were fixed and RABV N protein (red), SG marker TIA-1 (green), and nuclei (blue) were visualized using an indirect immunofluorescent assay. (B) Quantification of the numbers of SG (TIA-1)-forming cells infected with RABV (MOI of 1, 24 hpi). More than 300 cells in three random fields were analyzed per sample (n = 3), and the results are means and SE. *, significant difference ($P < 0.05$); ns, no significant difference. (C) TIAR and (D) G3BP1 were stained as SG marker proteins in Nishigahara- or Ni-CE-infected 293T cells (MOI of 1; 24 hpi). (E) 293T cells were infected with RABV street strains 1088 and Komatsugawa at an MOI of 0.03. At 24 hpi, cells were fixed, and RABV N protein (red), TIAR (green), and nuclei (blue) were visualized using an indirect immunofluorescent assay. Bars, 20 μm.

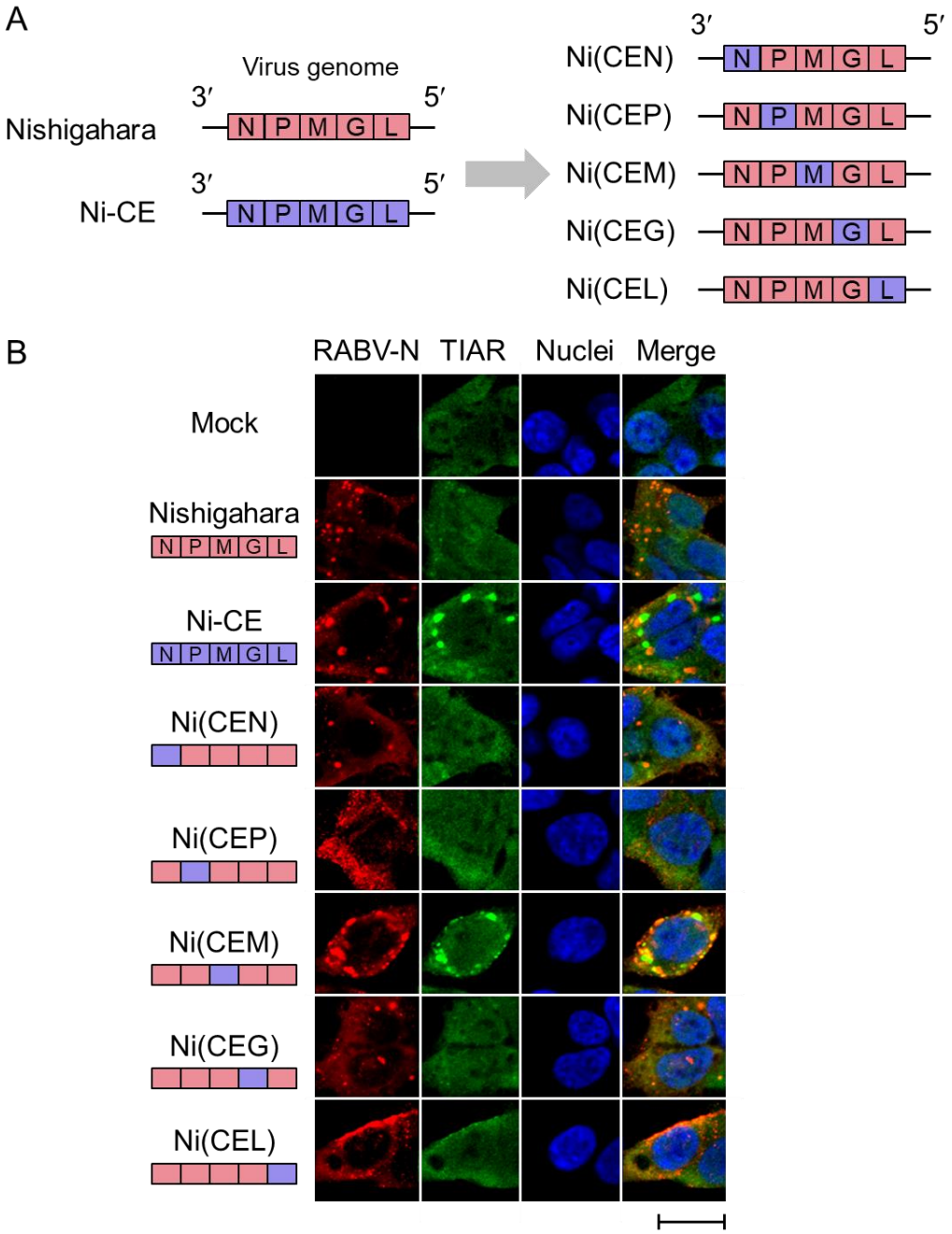

Fig.1-2. Analyses of the responsible RABV protein to inhibit SG formation. (A) Schematic diagram of the genome organization of the Nishigahara, Ni-CE, and chimeric virus strain (the latter were established by replacement of an Ni-CE strain gene with its Nishigahara genome background equivalent). The red and blue boxes represent RABV protein gene derived from the Nishigahara or the Ni-CE strains, respectively. (B) The M protein of Ni-CE is a determinant of induction of SG formation. 293T cells were infected with the Nishigahara, Ni-CE, or a chimeric virus strain (the latter were established by replacement of an Ni-CE strain gene with its Nishigahara genome background equivalent) at an MOI of 1. At 24 hpi, cells were fixed and RABV-N (red), SG marker TIAR (green), and nuclei (blue) were stained. Bar, 20 μm.

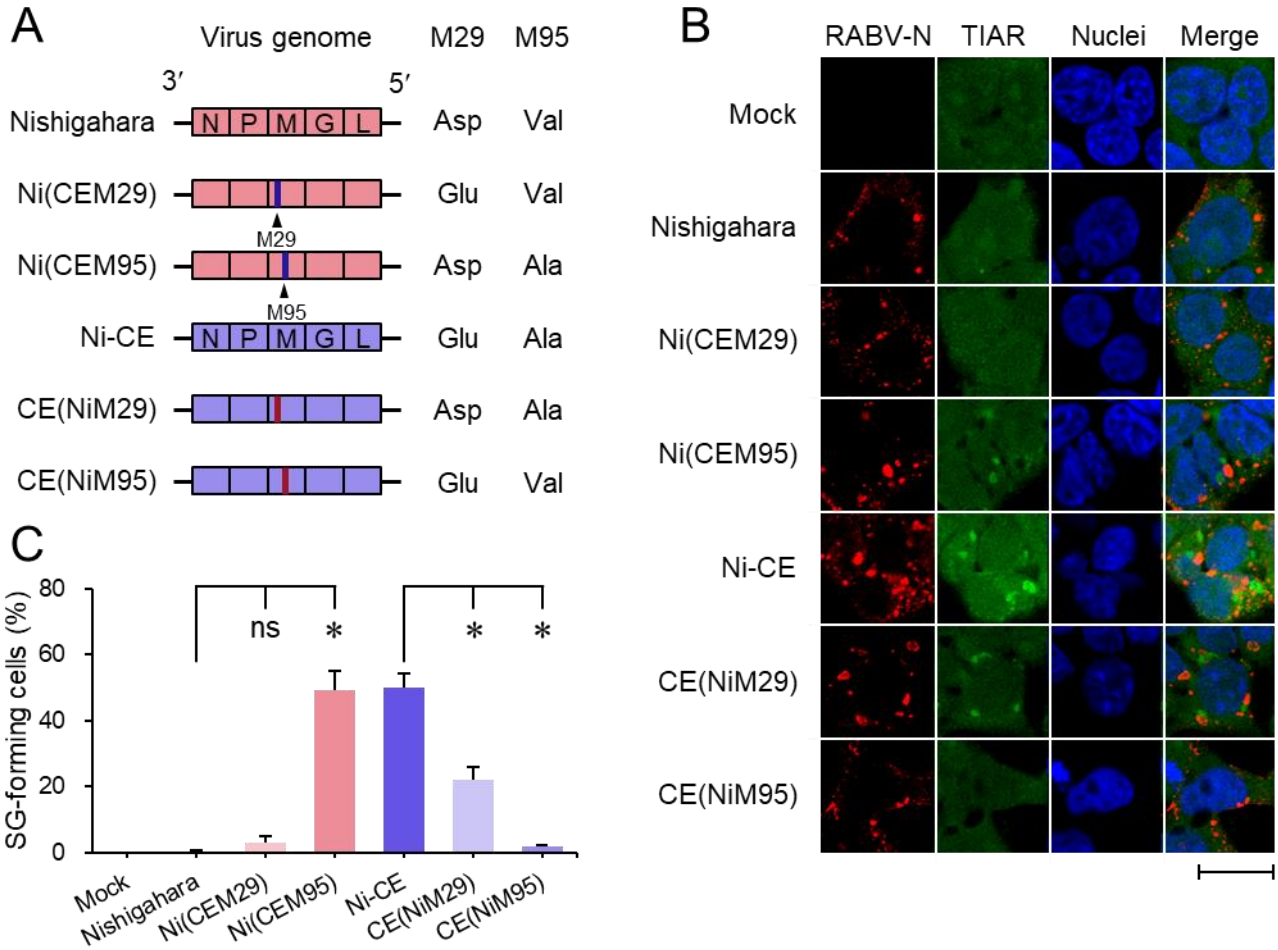

Fig.1-3. Analyses of the responsible amino acid in M protein to inhibit SG formation. (A) Schematic diagram of the genome organization of Nishigahara, Ni-CE, and M29-mutated strains [Ni(CEM29) or CE(NiM29)] or M95-mutated strains [Ni(CEM95) and CE(NiM95)]. The red and blue lines represent M29 and M95 derived from Nishigahara and Ni-CE, respectively. (B) Investigation of M protein amino acids related to SGformation.293T cells were infected with Nishigahara, Ni-CE, an M29-mutated strain, or an M95-mutated strain at an MOI of 1. At 24 hpi, cells were fixed, and RABV N (red), TIAR (green), and nuclei (blue) were stained. Bar, 20 mm. (C) Quantification of SG-forming cells infected with each RABV strain. More than 300 cells in three random fields were analyzed per sample (n =3), and the results are means and SE. *, significant difference ($P < 0.05$); ns, no significant difference.

Chapter II

Mechanism of stress granule formation related to the amino acid at position 95 in rabies virus matrix protein

INTRODUCTION

In chapter I, I elucidated that M95 is the important factor to inhibit SG formation, while the mechanism of SG formation induced by Ni-CE strain has not fully understood. Canonical SG formation is triggered by stress, and one such trigger is a viral infection. Entry of a virus into a cell can result in phosphorylation of eukaryotic translation initiation factor 2 α (eIF2α), and phosphorylated-eIF2α (p-eIF2α) then activates SG formation in the cytoplasm (54). The four cellular kinases known to be involved in eIF2α phosphorylation are protein kinase R (PKR), general control nonderepressible 2 (GCN2), PKR-like endoplasmic reticulum kinase (PERK), and heme-regulated inhibitor (HRI) (55).

Researchers have recently elucidated the role of SGs in innate antiviral immunity, which represents a notable addition to their previously known roles in storing mRNA and aberrant proteins, and repressing translation. The activation of this innate antiviral immunity crucially relies on SGs functioning as a platform (25–28). The relevant innate immune signaling is initiated when PKR, which phosphorylates eIF2α, recognizes viral double-stranded RNA (dsRNA) (25, 56). The SG nucleator protein G3BP1 also promotes both inflammatory and interferon (IFN) responses (57). PKR and G3BP1 are involved in

the positive regulation of innate immune sensors, such as RIG-I (58, 59). Furthermore, RIG-I localizes in SGs induced by viral RNA, initiating IFN responses (60, 61).

For some viruses, suppressing SG formation in infected cells is a strategy to avoid triggering an innate immune response in the host. Nonstructural protein 1 (NS1) of the influenza A virus plays an important role in inhibiting SG formation through its action on either SG component proteins or PKR, resulting in reduced IFN expression and enhanced viral replication (60, 62, 63). On the other hand, VP35 of the Ebola virus blocks SG formation by interacting with G3BP1 (64, 65). Thus, several viruses are now recognized as being able to evade innate immunity through suppression of SG formation, which contributes to heightened virulence.

Recently, Nikolic *et al.* demonstrated that PKR silencing decreased SG formation and IFN-β transcription, promoting viral replication (46). Thus, SGs are suggested to have an inhibitory effect on RABV replication. However, the relation between the antiviral response via SG formation and RABV virulence is not fully understood in the absence of research comparing SG formation between virulent and avirulent strains.

Accordingly, in this chapter II, I investigated the mechanism induced by the Ni-CE strain. I found that this mechanism is involved in the PKR activation, eIF2α phosphorylation, and the RIG-I accumulation in SGs, which results in the IFN-β initiation.

MATERIALS AND METHODS

Cells

293T cells and NA cells were maintained regarding to the chapter I. Human cervical cancer HeLa cells were maintained in Dulbecco's modified MEM supplemented with 10% FCS and 1% penicillin-streptomycin-amphotericin B suspension. These cells were cultured at 37°C in a humidified 5% CO_2 atmosphere.

Viruses

Nishigahara, Ni-CE, chimeric and mutant strains used in this study were recovered using reverse genetics system regarding to the chapter I. Sendai virus (SeV) Cantell strain was propagated in 10-day-old chicken embryos and allantoic fluid was harvested at 72 hpi. The SeV titer was determined using a hemagglutinin test (HA) and 0.5% chicken erythrocytes.

Plasmids

Plasmids expressing the M protein from Nishigahara and Ni-CE strains (pCAGGS-NiM and pCAGGS-CEM, respectively) were generated in the mammalian expression

plasmid pCAGGS/MCS (66). A QuickChange Site-Directed Mutagenesis Kit (Agilent Technology, Santa Clara, CA, USA) was used to generate plasmids expressing the single point-mutated M proteins pCAGGS-NiM-95A and pCAGGS-CEM-95V, in which the amino acid at position 95 of the M protein from Nishigahara and Ni-CE strains was replaced with that of the Ni-CE and Nishigahara M protein, respectively.

Plasmids used for genome editing, pX330-U6-Chimeric_BB-CBh-hSpCas9 (pX330) and pSpCas9(BB)-2A-GFP (pX458), were obtained from Addgene (#42230 and #48138, respectively). pX330-PuroR, a puromycin-resistant gene expressing pX330 was generated by inserting a T2A-Puro cassette into the C-terminus of the SpCas9 gene of pX330.

Genome-edited cell lines provided by Dr. Takashi Fujita (Kyoto University) were generated as descried bellow: PKR-deficient Hera cells (PKR KO HeLa) were generated from pX458-PKR, which had been generated in turn by inserting guide RNA sequences of human PKR into pX458. PKR-deficient 293T cells (293TΔPKR) were generated from pX330-PuroR/hPKR#1 and pX330-PuroR/hPKR#2, and G3BP1-deficient 293T cells (293TΔG3BP1) were generated from pX330-PuroR/hG3BP1#1 and pX330-PuroR/hG3BP1#2. PuroR/hPKR#1, pX330-PuroR/hPKR#2, pX330-PuroR/hG3BP1#1, and pX330-PuroR/hG3BP1#2 were generated in turn by inserting guide RNA sequences

of human PKR into pX330-PuroR. The sgRNA sequences for each target are shown in Table 2-1.

Genome editing

293T cells were cultured in a 24-well plate at 2.0×10^5 cells per well and transfected with 0.5 μg/well of pX330-PuroR/hPKR#1 and pX330-PuroR/hPKR#2, or 0.5 μg/well of pX330-PuroR/hG3BP1#1 and pX330-PuroR/hG3BP1#2, using polyethyleneimine "Max" (Polysciences Inc., Warrington, PA, USA). Transfected cells were transferred to a 100 mm dish at 5.0×10^2 cells, and subject to puromycin selection (20 μg/ml). Selected cells were cloned and confirmed to express PKR or G3BP1 protein by western blotting, as described below.

PKR KO HeLa cells were established by using pX458-PKR. GyrB-PKR HeLa cells, which transiently form SGs upon drug (coumermycin A1) administration, were generated by co-transfection with the GyrB-PKR expression vector and selection marker plasmid pIRES puro2 (Clontech, Mountainview, CA, USA) into PKR KO HeLa cells. At 48 hours after transfection, cells were selected for puromycin (InvivoGen, San Diego, CA, USA) resistance for two weeks, followed by single-cell selection.

Indirect immunofluorescent staining

Cells were cultured, infected, fixd, and stained regarding to the chapter I. For analysis of RIG-I accumulation in SGs, an anti-RIG-I rabbit polyclonal antibody was used (60). After washing with phosphate-buffered saline (PBS), secondary antibody solution containing Dylight 594 anti-mouse IgG horse antibody (1:2,000, Vector Laboratories), Dylight 488 anti-goat IgG horse antibody (1:2,000, Vector Laboratories), and Hoechst 33342 (1:2,000, DOJINDO Laboratories) were added to each well, followed by incubation at 37°C for 1 h. Cells were mounted and analyzed regarding to the chapter I. For detection of p-eIF2α, anti-p-eIF2α rabbit mAb (1:500, #9721, Cell signaling, Danvers, MA, USA), Dylight 594 anti-rabbit IgG horse antibody (1:2,000, Vector Laboratories), and Alexa 405 anti-mouse IgG donkey antibody (1:2,000, Abcam, Cambridge, UK) were used. Anti-SeV rabbit polyclonal antibody (1:2,000, pAb; MBL, Aichi, Japan) and anti-RABV-M protein mouse mAb (1:8,000, #53-D-33; kindly provided by Dr. Akira Nishizono, Oita University) were used to stain SeV-infected cells and RABV-M-expressing cells, respectively.

Western blotting

Cells (293T, 293TΔPKR, and 293TΔG3BP1) infected with the relevant RABV strain at an MOI of 1 at 24 hpi were lysed with RIPA buffer [50 mM Tris-HCl (pH 7.5), 150 mM NaCl, 1 mM EDTA, 1% NP-40, 0.5% sodium deoxycholate] including Protease Inhibitor Cocktail (Nacalai Tesque, Kyoto, Japan). After incubation on ice for 15 min, cell lysates were centrifuged (12,000 × *g*, 10 min, 4°C), and the lysate supernatant was mixed with an equal amount of 2× sodium dodecyl sulfate-polyacrylamide gel electrophoresis (SDS-PAGE) sample buffer [125 mM Tris-HCl (pH6.8), 4% SDS, 20% (w/v) glycerol, 0.01% bromophenol blue, and 10% (v/v) 2-mercaptoethanol]. After incubation at 95°C for 5 min, proteins in the samples were electrophoretically separated using a 10% acrylamide gel before transfer onto Immobilon-P membranes (Merck Millipore, Burlington, MA, USA). The membranes were blocked using Blocking One (Nacalai Tesque) reagent, except for p-eIF2α detection, Blocking One P (Nacalai Tesque) was used. The membranes were then incubated with anti-p-eIF2α rabbit mAb (1:500, #9721, Cell signaling), anti-eIF2α rabbit antibody (1:500, #sc-11386, Santa Cruz Biotechnology), anti-PKR goat antibody (1:500, #18244-1-AP, Proteintech, Rosemont, IL), anti-G3BP1 goat antibody (1:500, #sc-70283, Santa Cruz Biotechnology), anti-RABV N mouse mAb (1:10,000), anti-RABV-M mAb (1:8,000), or an anti-tubulin

mouse mAb (1:5,000, T5168; Sigma Aldrich, Saint Lois, MI, USA) diluted with tris-buffered saline (TBS) containing 0.1% Tween-20. For the secondary antibody, HRP-conjugated anti-mouse IgG (1:5,000, P0260, Dako, Glostrup, Denmark), anti-rabbit IgG (1:5,000, P0448, Dako), or anti-goat IgG (1:5,000, P0449, Dako) was used. Protein bands were visualized by using ECL Prime Western Blotting Detection Reagent (GE Healthcare, Chicago, IL, USA) and images were recorded using an ImageQuant LAS 500 (GE Healthcare). The intensities of the protein bands were quantified with Fiji image processing software (https://imagej.net/software/fiji/).

Assessment of RABV-M expression effects on SG formation

Cells were cultured in an 8-well chamber slide at 1.0×10^5 cells per well and transfected with 0.25 μg of pCAGGS-NiM, pCAGGS-CEM, pCAGGS-NiM-95A, pCAGGS-CEM-95V, or empty vector pCAGGS/MCS, using polyethyleneimine “Max.” In the experiment to examine whether M protein alone induces SG formation, cells were fixed 24 h post-transfection. In an experiment to examine the ability of M protein expression alone to inhibit SG formation, cells were infected with SeV (2,000 HA units/well) at 24 h post-transfection and fixed at 24 hpi. Cells were then observed by

indirect fluorescent-antibody staining for M protein and TIAR by the method described above.

Quantification of SG-forming cells using transient SG-inducible cells.

293T cells, 293TΔPKR, 293TΔG3BP, and GyrB-PKR HeLa cells were cultured in an 8-well chamber slide at 1.0×10^5 cells per well. 293T, 293TΔPKR, 293TΔG3BP cells were infected with Nishigahara, Ni-CE, M29-mutanted, or M95-mutated strain at MOI of 1 and fixed at 24hpi. GyrB-PKR HeLa cells were transfected with 0.25 μg of pCAGGS-NiM, pCAGGS-CEM, pCAGGS-NiM-95A, or pCAGGS-CEM-95V, and exposed to 10 nM coumermycin A1 (Promega, Madison, WI, USA) for 2 h at 24 h post-transfection. Dimethyl sulfoxide (DMSO) was used as the negative control. Cells were then fixed and stained for observing SG formation as described above. The numbers of SG-forming and RABV-infected or RABV-M expressing cells were counted with the aid of a confocal laser scanning microscope. More than 100 or 300 cells in three random fields were analyzed per sample and the results are expressed as means and SE.

Quantitative reverse transcription-polymerase chain reaction (qRT-PCR)

Cells were cultured in a 24-well plate at 2.0×10^5 cells per well and infected with the Nishigahara, Ni-CE, Ni(CEM95), or CE(NiM95) strain at an MOI of 1. At 24 hpi, total RNA extraction was performed by using an InnuPREP RNA Mini kit (Analytik Jena, Jena, Germany), followed by reverse transcription using a GeneAce cDNA Synthesis Kit (Nippon Gene, Tokyo, Japan). Real-time PCR was performed using CFX Connect (Bio-Rad, Hercules, CA, USA) and Thunderbird SYBR qPCR Mix (TOYOBO, Osaka, Japan). Primer sequences are shown in Table 2-1. Data are expressed as the number of copies of specific mRNA per copy of human housekeeping glyceraldehyde 3-phosphate dehydrogenase (*GAPDH*) mRNA. All assays were carried out in triplicate and the results are expressed as means and SE.

Statistical analysis

Statistical significance was evaluated using the Student *t*-test for two-group comparisons and one-way analysis of variance, followed by Tukey's test for multiple-group comparisons. Values of $P < 0.05$ were regarded as significant.

RESULTS

The amino acid at position 95 in the RABV-M protein plays a critical role in eIF2α phosphorylation in infected cells

Since SG formation is accelerated by eIF2α phosphorylation (54), I investigated p-eIF2α in cells infected with Nishigahara, Ni-CE, Ni(CEM95), and CE(NiM95) strains to elucidate whether phosphorylation of eIF2α is involved in M95-related induction of SG formation. Cells infected with the Nishigahara or CE(NiM95) strain did not show p-eIF2α in the indirect immunofluorescent assay, whereas cells infected with the Ni-CE or Ni(CEM95) strain showed a marked p-eIF2α signal, with diffuse staining in the cytoplasm (Fig. 2-1A).

Western blotting was performed to measure p-eIF2α levels in cells infected with one of the strains used for evaluation (Fig. 2-1B). Consistent with the results from the indirect immunofluorescent assay (Fig. 2-1A), the signal level of p-eIF2α normalized for tubulin was increased in cells infected with the Ni-CE and Ni(CEM95) strains, relative to that of uninfected cells. In contrast, no increase in the p-eIF2α level was observed in cells infected with the Nishigahara or CE(NiM95) strain (Fig. 2-1B). These results indicate that the mutation at M95 from Val to Ala is important for eIF2α phosphorylation.

Importance of PKR and G3BP1 for SG formation in Ni-CE strain-infected cells

Since Nikolic *et al*. reported that knockdown of PKR strongly impaired induction of SG formation in RABV CVS strain-infected cells (46), PKR has been speculated to play an important role in RABV-inducible SG formation. On the other hand, G3BP1 also plays a key role in SG formation, working with PKR, in several virus infections (25, 57, 67). Accordingly, to investigate the importance of PKR and G3BP1 in SG formation induced by the Ni-CE strain, we established 293TΔPKR and 293TΔG3BP1 cells by knocking out the genes encoding PKR and G3BP1 using the CRISPR/Cas9 system. Among Ni-CE-infected cells, 293TΔPKR and 293TΔG3BP1 cells showed fewer SGs than 293T cells (Figs. 2-2A and 2-2B). Western blotting results revealed the detection of p-eIF2α in 293T and 293TΔG3BP1 cells infected with the Ni-CE strain, but not in 293TΔPKR cells (Fig. 2-2C). These results indicate that both PKR and G3BP1 play an important role in SG formation induced by the Ni-CE strain.

Expression of the Nishigahara or Ni-CE M protein neither facilitates nor inhibits SG formation

To reveal the effect of the expression of M protein on SG formation, I investigated SG formation in 293T cells transfected with plasmids expressing the M protein of the Nishigahara or Ni-CE strain, or a mutant M protein with a substitution at M95 between the Nishigahara and Ni-CE strains (NiM, CEM, NiM-95A, and CEM-95V). Although I observed cells expressing RABV-M protein at 24 h post-transfection, no SG formation was observed in any plasmid-transfected cells (Fig. 2-3A). These results suggest that none of the investigated M proteins induced SG formation.

To determine whether the expression of a single M protein can inhibit SG formation caused by an exogenous viral infection, I next investigated SG formation in RABV-M expressing cells infected with SeV, which strongly induces SG formation (68). At 24 hpi, all SeV-infected cells formed SGs regardless of RABV-M expression (Fig. 2-3B), suggesting that none of the investigated M proteins inhibits SG formation.

To investigate whether the RABV-M protein inhibits SG formation in a PKR activation-dependent manner, I used GyrB-PKR HeLa cells, which express a PKR protein fused to Gyrase-B and in which PKR is activated in the presence of coumermycin A1, resulting in SG formation. GyrB-PKR HeLa cells were transfected with plasmids

expressing NiM, CEM, NiM-95A, CEM-95V, and empty vector. At 24 h post-transfection, cells were exposed to coumermycin A1, and SG formation was examined using a confocal microscope. As expected, all cells exposed to coumermycin A1 showed significantly more SG formation than that of cells exposed to DMSO. Notably, consistent with the results for SeV-infected cells (Fig. 2-3B), cells expressing the M protein of the Nishigahara and Ni-CE strains or their mutants showed no difference in the efficiency of SG formation (Fig. 2-3C and 2-3D). These results suggest that the expression of the Nishigahara or Ni-CE M protein neither facilitates nor inhibits SG formation.

SGs induced by Ni-CE, Ni(CEM), and Ni(CEM95) infection act as platforms for activation of the antiviral response

SGs act as platforms in the activation of RIG-I, which is an important viral RNA sensor for initiating antiviral responses (26, 30). RIG-I is reportedly accumulated and activated in SGs by interacting with PKR and G3BP1 (26, 69), and activated RIG-I then initiates IFN-β production (31, 70). Therefore, to elucidate the effects of SGs induced by the Ni-CE strain, I investigated RIG-I accumulation in SGs and IFN-β transcription levels in cells infected with the Nishigahara strain, Ni-CE strain, Nishigahara chimeric viruses, or M95-mutated strains (Fig. 2-4). Cells infected with the Nishigahara, Ni(CEN),

Ni(CEP), Ni(CEG), or Ni(CEL) strain did not show RIG-I accumulation in SGs at 24 hpi, whereas cells infected with the Ni-CE or Ni(CEM) strain showed strong RIG-I accumulation in SGs (Fig. 2-4A). Furthermore, although cells infected with the Nishigahara or CE(NiM95) strain did not show RIG-I accumulation in SGs at 24 hpi, cells infected with Ni-CE or Ni(CEM95) did (Fig. 2-4B). These results suggest that RIG-I accumulation in SGs is inducible in cells infected with the Ni-CE, Ni(CEM), or Ni(CEM95) strain—where M95 is occupied by Ala. Notably, cells infected with the Ni-CE or Ni(CEM95) strain showed a higher quantity of *IFN-β* mRNA than that of cells infected with the CE(NiM95) or Nishigahara strain (Fig. 2-4C). These results suggest that RABV M95-related induction of SGs facilitates activation of RIG-I, which initiates *IFN-β* mRNA transcription.

DISCUSSION

When cells are infected with viruses, SGs form, suppressing viral replication and inducing antiviral responses (25, 26). Cells infected with RABV also form SGs, but neither the RABV protein responsible for SG formation nor the effects of RABV-induced formation of SGs is fully understood (46). In this chapter, I demonstrated that M95, the known pathogenic determinant of the Nishigahara strain (39), plays a critical role in inhibiting SG formation through PKR activation, eIF2α phosphorylation, and subsequent RIG-I accumulation, which results in inhibiting the initiation of IFN-β.

I showed that the mutation at M95 from Val to Ala is associated with SG generation induced by PKR activation and eIF2α phosphorylation (Figs. 2-1 and 2-2). PKR acts as a crossroad in viral sensing, innate immune signaling, and stress response pathways, ultimately activating the induction of IFN-β that occurs following the induction of SG formation. To counter this host response, many viruses have evolved to inhibit PKR activation (46, 71–73). Hepatitis C virus suppresses PKR by directly inhibiting the kinase function (71). Reovirus and vaccinia virus inhibit PKR by shielding dsRNA from PKR detection (72, 73). Thus, the Nishigahara strain, like hepatitis C virus, reovirus, and vaccinia virus, has the ability to inhibit SG formation induced by eIF2α phosphorylation,

whereas the Ni-CE strain may lack such ability. The Ni-CE strain is a long-term passaged strain of chicken embryo fibroblasts (40). Interestingly, chickens are genetically deficient in RIG-I (74), and the Ni-CE strain may have been passaged in an environment with no selection pressure for counteracting RIG-I-mediated innate immune signals; consequently it lost its ability to suppress RIG-I activation.

On the other hand, 293TΔG3BP1 cells infected with the Ni-CE strain formed fewer SGs than did wild-type 293T cells infected with the Ni-CE strain (Fig. 2-2), indicating that G3BP1 also plays an important role when SG formation is induced by Ni-CE infection. G3BP1 binds directly to RIG-I, promoting IFN-transcription initiated by RIG-I activation; the binding has been suggested to be blocked or cleaved by some viruses, as an evolutionarily acquired strategy to inhibit SG formation (65, 69, 75). The accumulation of RIG-I in SGs induced by Ni-CE infection suggests that the binding of G3BP1 to RIG-I plays an important role in innate immune activation in RABV-infected cells (Fig. 2-4). However, further studies are needed to clarify the details.

Some studies reported that the expression of a single viral protein inhibits SG formation (62, 63, 76–78). The expression of the NS1 protein of influenza A virus or the p4a protein of Middle East respiratory syndrome coronavirus plays a critical role in inhibiting SG formation by shielding viral dsRNA from PKR-detection (62, 63, 76, 77).

In this chapter, we demonstrated that the expression of RABV-M neither induces SG formation nor inhibits SG formation induced by SeV or PKR activation (Fig. 2-3). This suggests that the RABV-M protein is not directly related to SG formation in the manner of the NS1 and p4 proteins. Hence, the RABV-M protein may inhibit SG formation by cooperating with other RABV proteins.

In chapter I and II, I revealed that RABV-M protein plays an important role in SG formation induced by Ni-CE strain infection and represents the first report on the involvement of RABV-M protein in regulation of SGs (Fig. 1-2B). SGs induced by Ni-CE strain infection contain TIA-1, TIAR, and G3BP1, and they are localized near NBs and induced by PKR activation (Figs. 1-1 and 2-2). These results are consistent with those in previous reports demonstrating strong SG induction following infection with other RABV CVS strains (46). However, my findings also suggest that M95-mediated avoidance of SG formation induction may not be the dominant factor in the mechanism of virulence for the CVS strain. This view is based on the strong lethality to mice shown by the CVS strain after inoculation, and conservation of the amino acid (Val) at M95 across the CVS and Nishigahara strains. The Nishigahara strain, like the street strains, does not cause neuronal cell death (41), which is strongly induced by the CVS strain,

suggesting that the Nishigahara strain may be more characteristically similar to the street strain and thus a more appropriate model of street strains.

In summary, we demonstrated that M95 is a key determinant for SG formation induced by the Ni-CE strain through a mechanism related to PKR activation and eIF2α phosphorylation. The relevant action might be induced through the interaction between the M protein and other RABV proteins. However, the M protein cannot trigger SG in absence of infection. We further demonstrated that SGs induced by the Ni-CE strain act as a platform for the accumulation and activation of RIG-I, resulting in IFN-β transcription. We anticipate that the findings in this study will be useful in achieving a better understanding of the molecular mechanism behind RABV pathogenesis.

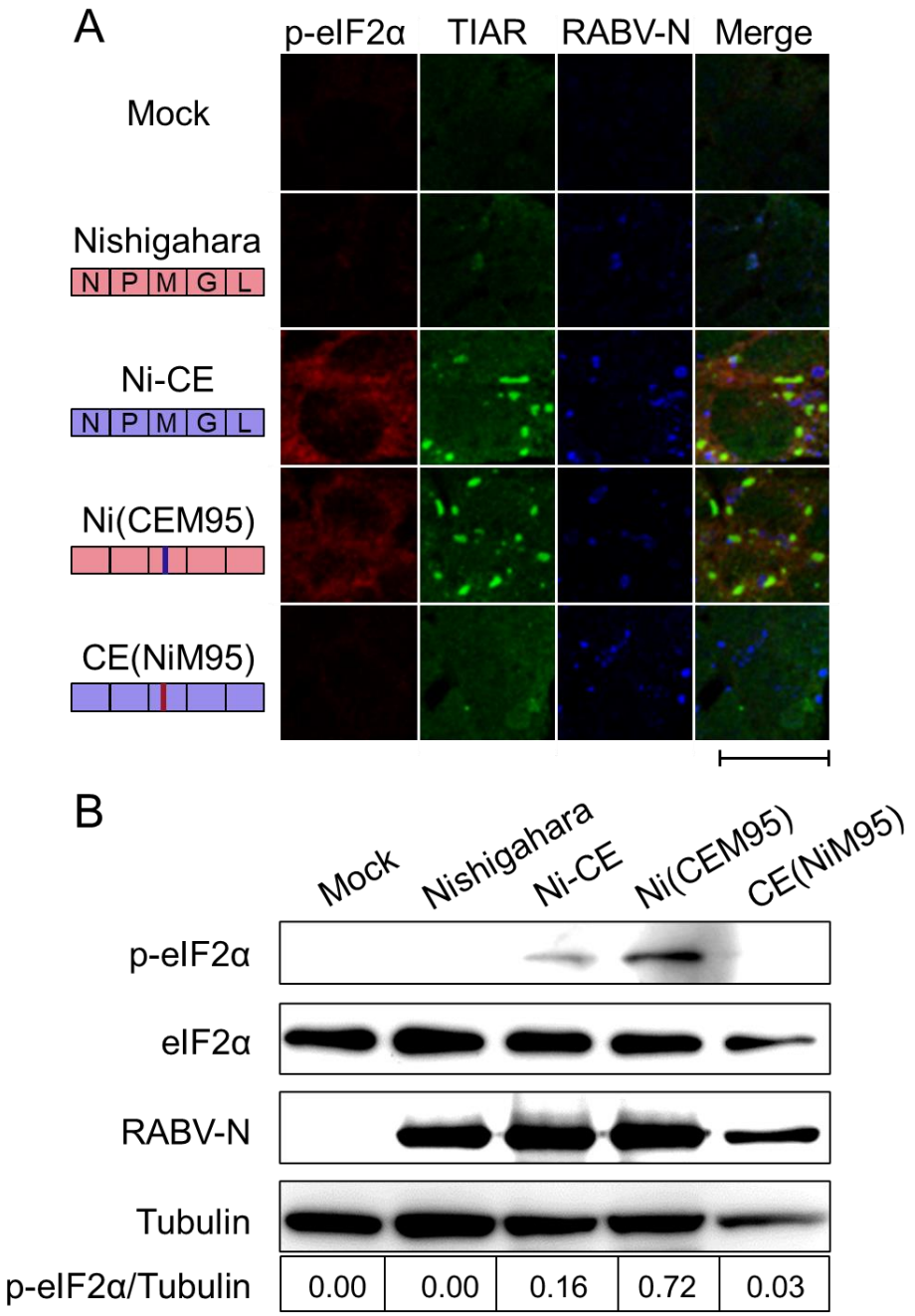

Fig. 2-1. Importance of the amino acid at position 95 of the M protein for phosphorylation of eIF2a (p-eIF2a). (A) Visualization of p-eIF2a in 293T cells infected with the Nishigahara, Ni-CE, or M95-mutated [Ni(CEM95) or CE(NiM95)] RABV strain at an MOI of 1. At 24 hpi, cells were fixed and p-eIF2a (red), TIAR (green), and RABV-N (blue) were stained. Bar, 10 μm. (B) Detection of p-eIF2a by western blotting in cells infected with the Nishigahara, Ni-CE, or M95-mutated RABV strain. 293T cells were infected with Nishigahara, Ni-CE, Ni(CEM95), or CE(NiM95) strain at an MOI of 1 and lysed at 24 hpi. Proteins were detected using antibodies against p-eIF2a, eIF2a, and RABV-N. Tubulin is shown as a loading control.

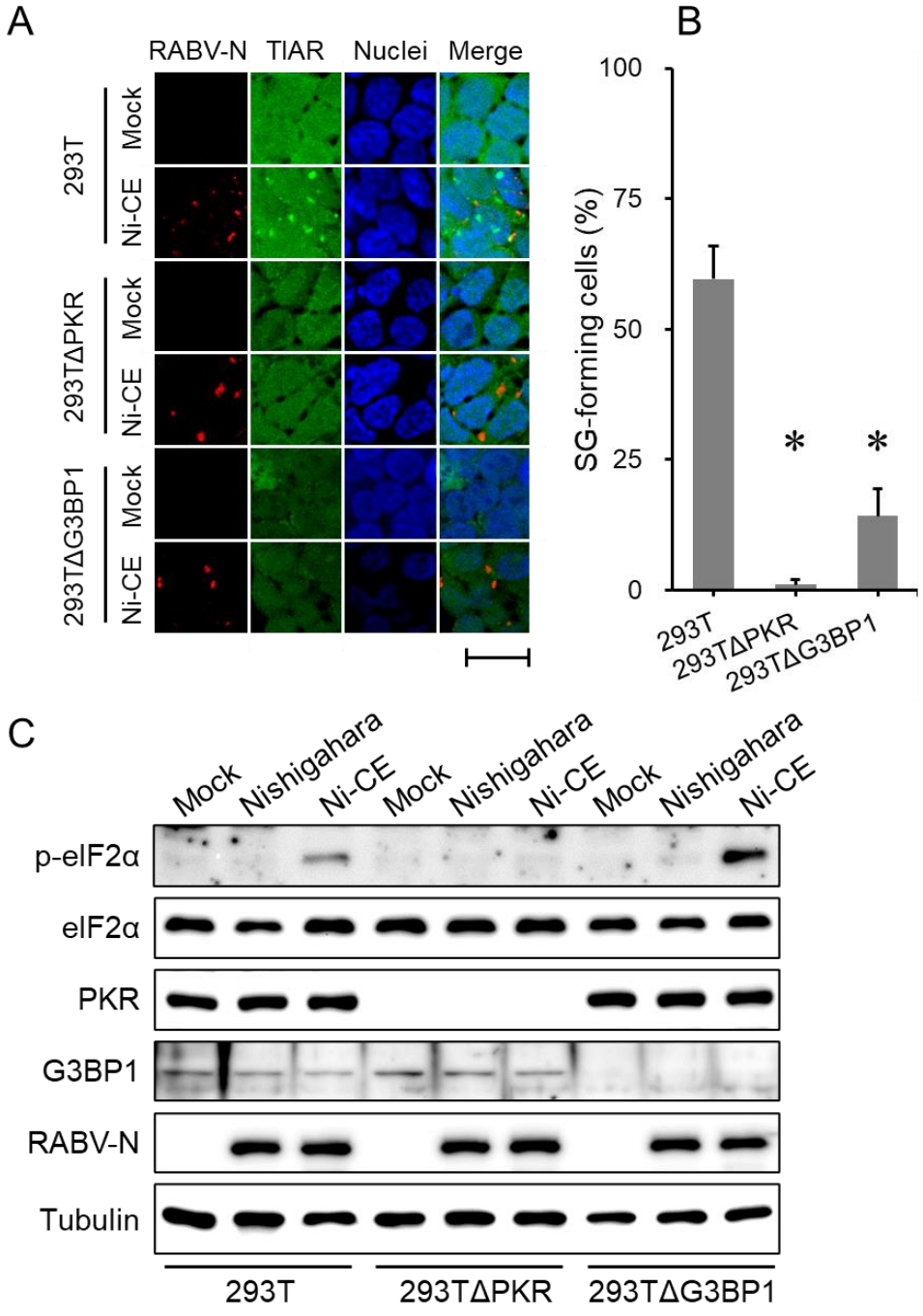
A
RABV-N
TIAR
Nuclei
Merge
293T
Mock
Ni-CE
293TΔPKR
Mock
Ni-CE
293TΔG3BP1
Mock
Ni-CE
B
SG-forming cells (%)
100
75
50
25
0
*
*
293T
293TΔPKR
293TΔG3BP1
C
Mock
Nishigahara
Ni-CE
Mock
Nishigahara
Ni-CE
Mock
Nishigahara
Ni-CE
p-eIF2α
eIF2α
PKR
G3BP1
RABV-N
Tubulin
293T
293TΔPKR
293TΔG3BP1

Fig. 2-2. Knockout effects of SG-related proteins PKR and G3BP1 on SG formation in Ni-CE-infected cells. (A) Visualization of SGs in 293T, 293TΔPKR, and 293TΔG3BP1 cells infected with mock or the Ni-CE strain at an MOI of 1. At 24 hpi, cells were fixed and RABV-N (red), TIAR (green), and nuclei (blue) were stained. Bar, 20 μm. (B) Reduction of SG formation in PKR or G3BP1 KO cells infected with the Ni-CE strain. 293T, 293TΔPKR, and 293TΔG3BP1 cells were infected with the Ni-CE strain at an MOI of 1. At 24 hpi, cells were fixed and TIAR and RABV-N proteins were co-stained to observe SG formation in infected cells. More than 100 Ni-CE-infected cells in three random fields were randomly observed using confocal microscopy, and the number of cells forming SGs in these fields was counted and the percentage determined. Results are expressed as means and SE. *; significant difference ($P < 0.05$). (C) Phosphorylation of eIF2a in 293T, 293TΔPKR, and 293TΔG3BP1 cells infected with mock, Nishigahara, or Ni-CE strains at an MOI of 1. At 24 hpi, cells were lysed and p-eIF2a, eIF2a, PKR, G3BP1, and RABV-N were detected by western blotting using specific antibodies. Tubulin is shown as a loading control.

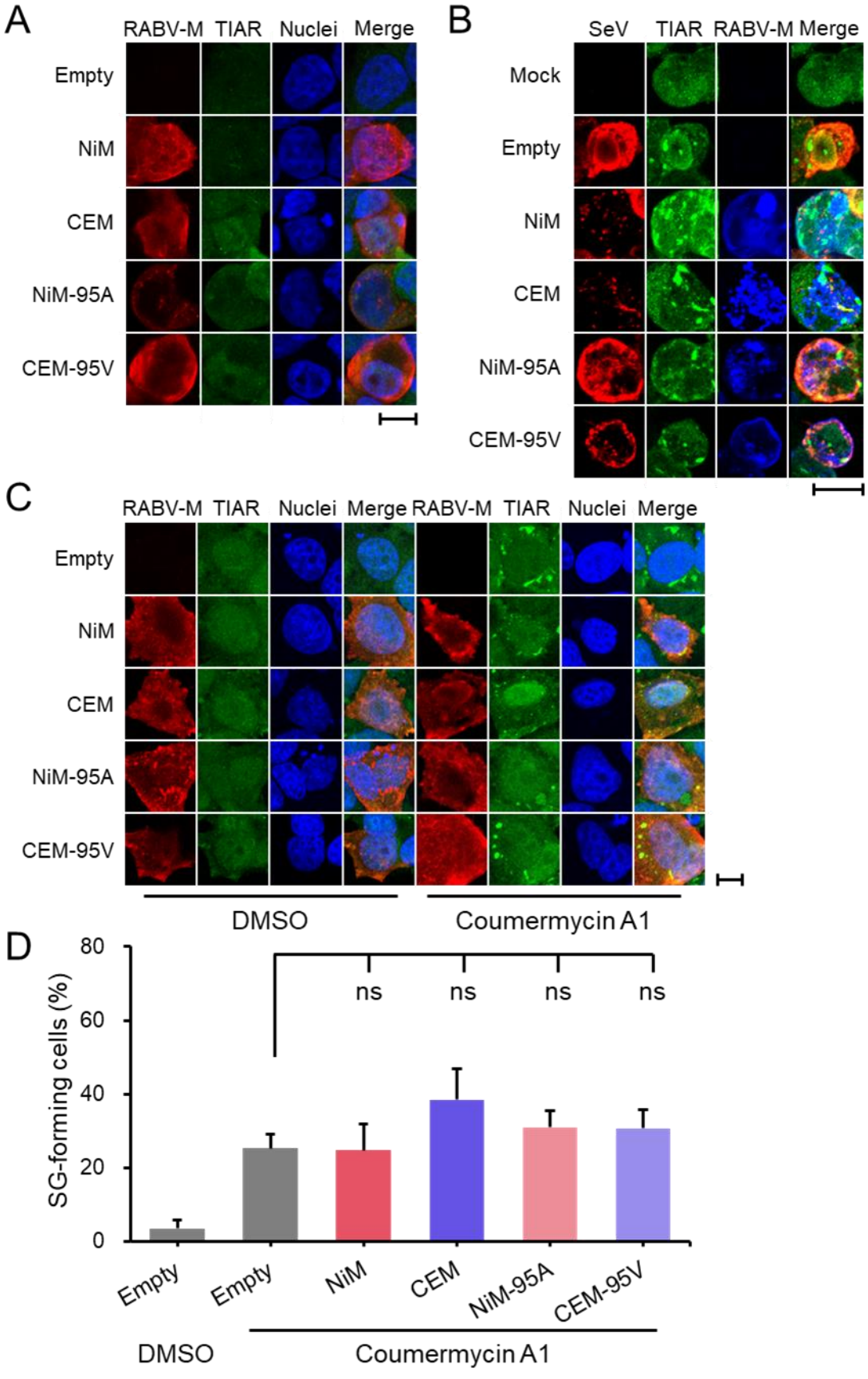
A
RABV-M
TIAR
Nuclei
Merge
Empty
NiM
CEM
NiM-95A
CEM-95V
B
SeV
TIAR
RABV-M
Merge
Mock
Empty
NiM
CEM
NiM-95A
CEM-95V
C
RABV-M
TIAR
Nuclei
Merge
RABV-M
TIAR
Nuclei
Merge
Empty
NiM
CEM
NiM-95A
CEM-95V
DMSO
Coumermycin A1
D
SG-forming cells (%)
80
60
40
20
0
ns
ns
ns
ns
Empty
Empty
NiM
CEM
NiM-95A
CEM-95V
DMSO
Coumermycin A1

Fig. 2-3. Assessment of RABV-M expression effects on SG formation. (A) Expression of RABV-M protein in the absence of stimulation of SG formation. 293T cells were transfected with 0.25 μg of pCAGGS-NiM, -CEM, -NiM-95A, or -CEM-95V. At 24 hours post-transfection, the cells were fixed and RABV-M (red), TIAR (green), and nuclei (blue) were stained. Bar, 10 μm. (B) A single expression of RABV-M in the presence of stimulated SG formation. 293T cells were transfected with 0.25 μg of pCAGGS-NiM, -CEM, -NiM-95A, or -CEM-95V. At 24 h post-transfection, the cells were infected with the Sendai virus (SeV) at 2,000 HA unit/well. At 24 hpi, the cells were fixed and SeV (red), TIAR (green), and RABV-M (blue) were stained. Bar, 10 μm. (C) A single expression of RABV-M in the presence of stimulated PKR activation. GyrB-PKR HeLa cells were transfected with 0.25 μg of pCAGGS-NiM, -CEM, -NiM-95A, and -CEM-95V. At 24 h post-transfection, cells were exposed to 10 nM coumermycin A1 for 2 h. DMSO was used as the negative control. The cells were then fixed and RABV-M (red), TIAR (green), and nuclei (blue) were stained. Bar, 10 μm. (D) SG-forming ratio in RABV-M expressing GyrB-PKR HeLa cells stimulated with coumermycin A1 as described in (C). GyrB-PKR HeLa cells were exposed to 10 nM coumermycin A1 for 2 h. DMSO was used as the negative control. The numbers of SG-forming and RABV-M expressing cells were counted with a confocal laser scanning microscope. More than 300 cells in three random fields were analyzed per sample and the results are expressed as means and SE. ns, no significant difference ($P > 0.05$).

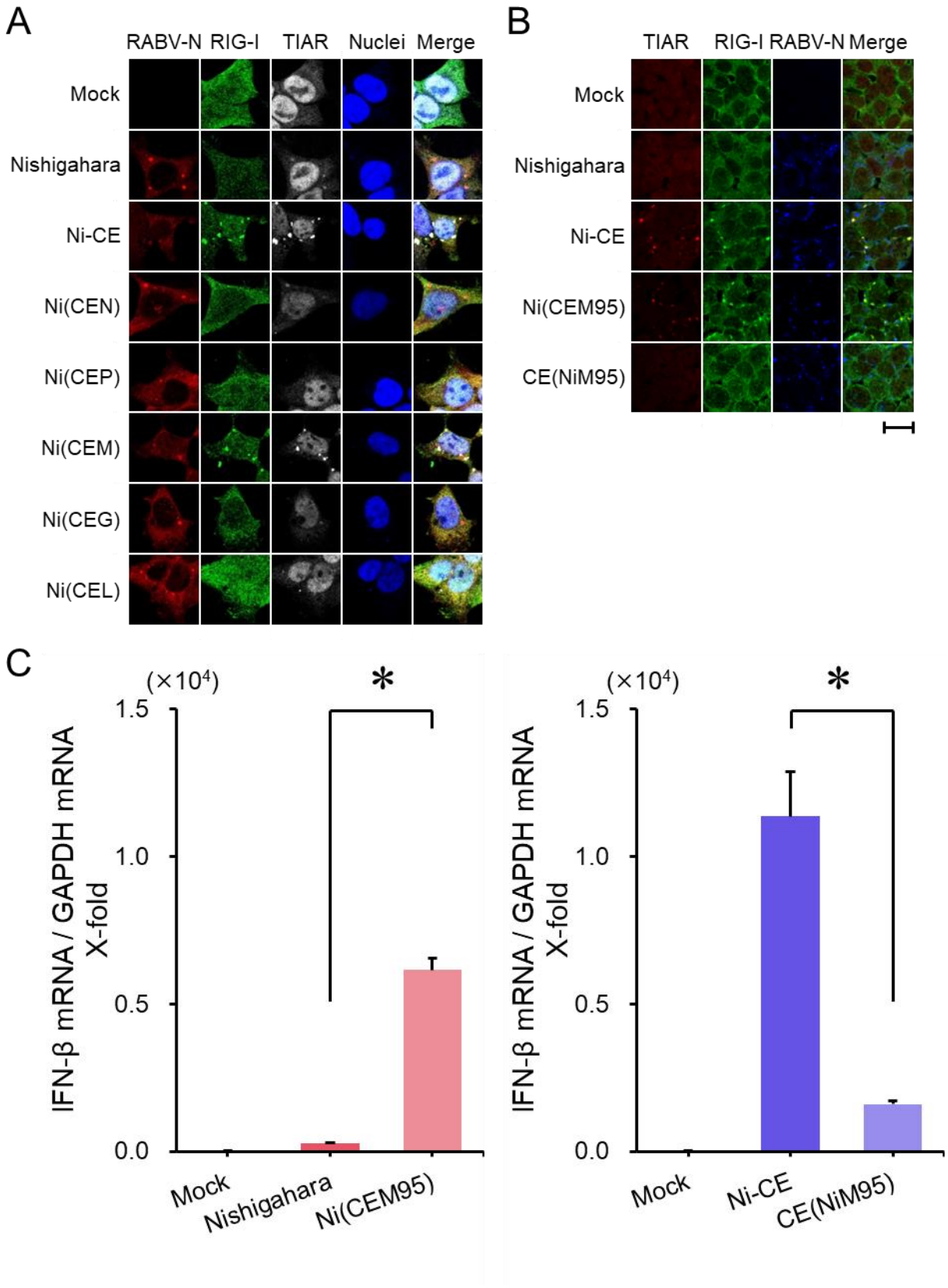
A
RABV-N
RIG-I
TIAR
Nuclei
Merge
Mock
Nishigahara
Ni-CE
Ni(CEN)
Ni(CEP)
Ni(CEM)
Ni(CEG)
Ni(CEL)
B
TIAR
RIG-I
RABV-N
Merge
Mock
Nishigahara
Ni-CE
Ni(CEM95)
CE(NiM95)
C
(×10⁴)
*
IFN-β mRNA / GAPDH mRNA
X-fold
1.5
1.0
0.5
0.0
Mock
Nishigahara
Ni(CEM95)
(×10⁴)
*
IFN-β mRNA / GAPDH mRNA
X-fold
1.5
1.0
0.5
0.0
Mock
Ni-CE
CE(NiM95)

Fig. 2-4. The M95 protein plays a critical role in RIG-I accumulation and the subsequent initiation of IFN-β transcription by RABV infection. (A) RIG-I localization in 293T cells infected with Nishigahara, Ni-CE, or a chimeric virus strain [Ni(CEN), Ni(CEP), Ni(CEM), Ni(CEG), or Ni(CEL); established by replacement of an Ni-CE strain gene with its Nishigahara genome background equivalent] at an MOI of 1. At 24 hpi, the cells were fixed and RABV-M (red), RIG-I (green), TIAR (white), and nuclei (blue) were stained. Bar, 20 μm. (B) RIG-I localization in 293T cells infected with the Nishigahara, Ni-CE, or M95-mutated strains Ni(CEM95) or CE(NiM95) at an MOI of 1. At 24 hpi, the cells were fixed and TIAR (red), RIG-I (green), and RABV-N (blue) were stained. Bar, 20 μm. (C) Comparison of IFN-β mRNA transcription level in 293T cells infected with the Nishigahara, Ni-CE, Ni(CEM95), or CE(NiM95) strain at an MOI of 1. At 24 hpi, total cellular RNA was extracted and reverse transcription performed. cDNA was analyzed for the expression level of human *IFN-β* using real-time PCR. Gene expression levels were normalized to human *GAPDH* mRNA levels. Each bar represents the means and SE of three technical replicates. *; significant difference ($P < 0.05$).

Table 2-1. Primers used in this chapter

Primer	Use	Sequence (5′-3′)
pX330-PuroR/hPKR#1 sgRNA forward	Knockout of PKR gene in 293T cells	CACCATTCAGGACCTCCACATGAT
pX330-PuroR/hPKR#1 sgRNA reverse		AAACATCATGTGGAGGTCCTGAAT
pX330-PuroR/hPKR#2 sgRNA forward	Knockout of PKR gene in 293T cells	CACCGTACTACTCCCTGCTTCTGA
pX330-PuroR/hPKR#2 sgRNA reverse		AAACTCAGAAGCAGGGAGTAGTAC
pX330-PuroR/hG3BP1#1 sgRNA forward	Knockout of G3BP1 gene in 293T cells	CACCGTATTACACACTGCTGAACC
pX330-PuroR/hG3BP1#1 sgRNA reverse		AAACGGTTCAGCAGTGTGTAATAC
pX330-PuroR/hG3BP1#2 sgRNA forward	Knockout of G3BP1 gene in 293T cells	CACCGCTTCTCTCTAACAACAACC
pX330-PuroR/hG3BP1#2 sgRNA reverse		AAACGGTTGTTGTTAGAGAGAAGC
pSpCas9(BB)-2A-GFP/hPKR sgRNA forward	Knockout of PKR gene in HeLa cells	CAGTGTGCATCGGGGGTGCAGTTT
pSpCas9(BB)-2A-GFP/hPKR sgRNA reverse		TGCACCCCCGATGCACACTGCGGTG
human IFN-β forward	Real-time PCR targeting IFN-β	GTCTGCACCTGAAAAGATATTATGG
human IFN-β reverse		CTGACTATGGTCCAGGCACA
human GAPDH forward	Real-time PCR targeting GAPDH	GCACCGTCAAGGCTGAGAAC
human GAPDH reverse		TGGTGAAGACGCCAGTGGA

Chapter III

Involvement of programmed cell death related to the amino acid at position 95 in rabies virus matrix protein

Introduction

In chapter I and II, I demonstrated that M95 plays a critical role in SG formation induced by Ni-CE infection, which results in the RIG-I accumulation and the initiation of IFN-β transcription. Recently, M95 has been reported to involve in RABV pathogenesis and programmed cell death. Previously report showed intracerebral inoculation of the CE(NiM95) strain, in which the Ala at M95 of Ni-CE strain was replaced with a Val from the M protein of the Nishigahara strain, was lethal in mice (39). Moreover, M95 Ala is required to induce cell death because the Ni-CE strain, but not the Nishigahara or CE(NiM95) strain, induces CPE characterized by cell rounding, shrinkage, and detachment in a mouse neuroblastoma cell line (41) (Fig. 3-1). In general, RABV virulent strains do not induce prominent inflammation and cell death in the central nervous system, whereas fixed, non-lethal strains induce these effects, implying that the pathogenicity of RABV is inversely correlated with inflammation and cell death (11, 52, 53). These previous studies suggest that the ability of M95 to induce cell death is correlated with the differences in the pathogenicity between the Nishigahara and Ni-CE strains; however, the intracellular signaling pathway involved in M95-induced cell death has not been elucidated.

It is reported that CPE induced by the Ni-CE strain was accompanied by the apoptosis-like characteristics of cell death, displaying cell rounding, shrinkage, and DNA fragmentation (41). Apoptosis is a physiological process of cell death characterized by specific morphological and biochemical changes (79). Caspases, a family of cysteine proteases, are prominent in apoptosis. Caspase-3 and -7 are well-known executioner caspases (80) that induce phosphatidylserine (PS) exposure, DNA fragmentation, and cell shrinkage (81, 82). Accordingly, apoptosis is defined as cell death caused by executioner caspases (33).

In this chapter, I aimed to elucidate the mechanisms by which M95 affects the cell death caused by RABV infection. I investigated cell death dynamics and apoptotic characteristics such as DNA fragmentation, activation of the executioner caspases, cell membrane disruption, and PS exposure in human neuroblastoma cells infected with the Nishigahara, Ni-CE, or M95-mutant strains.

MATERIALS AND METHODS

Cells and reagents

Human SK-N-SH neuroblastoma cells and NA neuroblastoma cells were maintained in E-MEM (Nissui) adjusted to pH 7.0 with $NaHCO_3$ and supplemented with 10% FCS and 1% penicillin-streptomycin-amphotericin B suspension (FUJIFILM Wako Pure Chemical,). Staurosporine (Sts; FUJIFILM Wako Pure Chemical) was used as an apoptosis inducer and Z-VAD-FMK (Peptide Institute, Ibaraki, Japan) was used as a caspase inhibitor.

Viruses

Nishigahara, Ni-CE, CE(NiM95), and Ni(CEM95) strains were recovered regarding to the chapter I. The fixed RABV strains CVS and ERA were also used as positive controls in this study. Stocks of all viruses were prepared in NA cells.

CPE observation

Monolayer of SK-N-SH cells in a 96-well plate (TPP, Trasadingen, Switzerland) were infected with each RABV strain at an MOI of 1. Morphological changes in infected

cells were observed with an inverted microscope (Eclipse Ti-S, Nikon, Tokyo, Japan) at 24, 48, and 72 hpi.

Cell viability assay

A Cell Titer-Glo 2.0 Cell Viability Assay Kit (Promega) was used to measure ATP luminescence as an indicator of metabolically active cells. Briefly, SK-N-SH cells were cultured in a 96-well white plate (Thermo Fisher Scientific) and infected with each RABV strain (MOI of 3). At 24, 48 and 72 hpi, equal volumes of the cell titer substrate buffer mixture and medium were added to each well. After shaking at room temperature for 1 min, luminescence was measured with a Glo-MAX Explorer Microplate Reader (Promega). Cells cultured with 1.0 μM Sts for 4–6 h were used as positive controls.

Terminal deoxynucleotidyl transferase-mediated dUTP nick-end labeling (TUNEL) assay

Apoptotic cells were detected by TUNEL assay using a MEBSTAIN Apoptosis TUNEL Kit III (MBL). Briefly, SK-N-SH cells grown on an 8-well chamber slide (SPL Life Sciences, Pocheon, South Korea) were infected with each RABV strain (MOI of 1). At 48 hpi, cells were fixed in PBS containing 4% paraformaldehyde (FUJIFILM Wako

Pure Chemicals) for 30 min. Subsequently, the cells were permeabilized with 100% methanol at room temperature for 1 min. Before TUNEL staining according to the manufacturer's instructions, the cells were incubated with anti-N mAb diluted in PBS at 37°C for 30 min. After washing five times with PBS, the slides were incubated with an Alexa Fluor 594-conjugated anti-mouse IgG secondary antibody (Invitrogen) diluted in PBS at 4°C overnight. After washing five times with PBS, the nuclei were stained by ProLong™ Diamond Antifade Mountant with DAPI (Invitrogen). Cells were examined using a BZ-X710 fluorescence microscope (Keyence, Osaka, Japan).

Real-time assessment of PS exposure and cell membrane disruption

Real-time assessment of PS exposure and cell membrane disruption as indicators of early and late apoptosis, respectively, was performed using a Real-Time-Glo Annexin V Apoptosis and Necrosis Assay (Promega) according to the manufacturer's instructions. Briefly, SK-N-SH cells were seeded into a 96-well white plate. After infection with each RABV strain (MOI of 3), cells were cultured in E-MEM containing the detection reagent, which had been prepared according to the manufacturer's instructions. Cells cultured in the same mixture containing 0.1 μM Sts were used as positive controls. The luminescence and fluorescence of the cultured cells were measured chronologically to evaluate PS

exposure and cell membrane disruption, respectively, at different time points using a Glo-MAX Explorer Microplate Reader.

Caspase-3/7 activity assay

The caspase-3/7 activity of RABV-infected cells was detected using a Caspase-Glo 3/7 Assay (Promega). SK-N-SH cells were cultured in 96-well plates and infected with each RABV strain (MOI of 1). At 36 and 48 hpi, the cells were lysed with Caspase-Glo buffer on ice for 10 min. Cells cultured with 1.0 μM Sts for 4–6 h were used as positive controls. Cell lysates were transferred into a 96-well white plate and the corresponding caspase substrate dissolved in Caspase-Glo buffer was added. After shaking at room temperature for 1 min, caspase-3/7 activity was measured as luminescence using a Glo-MAX Explorer Microplate Reader.

Western blotting

SK-N-SH cells were infected, lysed, collected supernatants, and mixed SDS-PAGE sample buffer regarding to the chapter II. After incubation at 95°C for 5 min, proteins in the samples were separated by 10% SDS-PAGE and then transferred onto Immobilon-P membranes (Merck Millipore). After blocking with PBS containing 5% skim milk

(FUJIFILM Wako Pure Chemicals) and 0.1% Tween-20 (FUJIFILM Wako Pure Chemicals), membranes were incubated at 4°C overnight with anti-poly (ADP-ribose) polymerase 1 (PARP-1) rabbit monoclonal antibody (#9542, Cell Signaling), anti-N mAb #13-27, or anti-tubulin mouse monoclonal antibody (T5168; Sigma Aldrich) diluted in PBS containing 1% skim milk and 0.1% Tween-20. After washing with PBS containing 0.1% Tween-20, the membranes were incubated at 37°C for 1 h with horseradish peroxidase-conjugated anti-mouse IgG (P0260, Dako) or anti-rabbit IgG (P0448, Dako) as the secondary antibody. Protein bands were visualized and images were acquired regarding to the chapter II.

Statistical analysis

Statistically significant differences between two groups were analyzed using Student's t-test and among multiple groups were analyzed using one-way analysis of variance, followed by Student–Newman–Keuls test. Values of $P < 0.05$ were regarded as significant.

RESULTS

Ni-CE and Ni(CEM95) strains induced stronger CPE and reduced cell viability in human neuroblastoma cells

To investigate whether the cell death induced by Ni-CE infection observed in mouse neuroblastoma NA cells (41) also occurred in other cell lines, we inoculated Nishigahara, Ni-CE, Ni(CEM95), and CE(NiM95) strains into human SK-N-SH neuroblastoma cells. I observed a stronger CPE in SK-N-SH cells infected with the Ni-CE and Ni(CEM95) strains than in those infected with Nishigahara and CE(NiM95) strains at 48 hpi (Fig. 3-2A); specifically, cells infected with the Ni-CE and Ni(CEM95) strains were more rounded, shrunken, and detached, resembling the response previously reported in NA cells. Furthermore, to determine whether CPE is related to cell death, I investigated cell viability by measuring ATP luminescence. SK-N-SH cells infected with the Ni-CE and Ni(CEM95) strains showed lower luminescence than cells infected with the Nishigahara and CE(NiM95) strains (Fig. 3-2B), demonstrating that the Ni-CE and Ni(CEM95) strains induced cell death more strongly. These results indicate that the M95 position is also related to the human SK-N-SH cell death induced by Ni-CE infection.

M95-related cell death also results in DNA fragmentation

A TUNEL assay to detected DNA fragmentation, a characteristic of apoptosis, was performed on SK-N-SH cells infected with each RABV strain. A greater proportion of TUNEL-positive cells were detected among SK-N-SH cells infected with the Ni-CE and Ni(CEM95) strains than among those infected with the Nishigahara and CE(NiM95) strains (Fig. 3-3). This result suggests that DNA fragmentation occurs during the process of cell death induced by Ni-CE infection.

M95-related cell death is involved in cell membrane disruption

To investigate the relationship between cell death induced by Ni-CE infection and the host cell membrane, I detected PS exposure and cell membrane disruption in real-time using SK-N-SH cells infected with each RABV strain. Luminescence and fluorescence (representing PS exposure and cell membrane disruption, respectively) were measured at different time points in the infected cells. Both Ni-CE- and Nishigahara-infected cells showed higher luminescence than mock-infected cells between 18 and 36 hpi, with comparable levels of luminescence (Fig. 3-4A, B, and C). Notably, after 36 hpi, luminescence decreased dramatically in Ni-CE-infected cells but not in Nishigahara-infected cells. In contrast, fluorescence levels were higher in Ni-CE-infected cells than in

Nishigahara-infected cells between 18 and 72 hpi. These results suggest that the Ni-CE strain induced cell membrane disruption and cell death through PS exposure, whereas Nishigahara strains did not induce cell membrane disruption despite PS exposure. Notably, Ni(CEM95)-infected and CE(NiM95)-infected cells showed the same dynamics of luminescence and fluorescence as those of Ni-CE-infected and Nishigahara-infected cells, respectively (Fig. 3-4D,E). These results indicate that M95 is strongly related to cell membrane disruption but not to PS exposure.

Activation of caspase-3/7 is involved in M95-related cell death for SK-N-SH cells

Apoptosis is induced by executioner caspases, mainly caspase-3, according to the definition of the Nomenclature Committee on Cell Death (33). Thus, I examined the activity of executioner caspases in SK-N-SH cells infected with each strain to clarify whether cell death induced by Ni-CE infection is associated with apoptosis. I demonstrated that the Ni-CE strain induced caspase-3/7 activity, in a similar manner to the positive control RABV strains (CVS and ERA) (13, 83), and this induced activity was significantly greater that seen with mock infection or the Nishigahara strain, in SK-N-SH cells (Fig. 3-5A). Notably, the Ni-CE and Ni(CEM95) strains induced higher caspase-3/7 activity than either mock infection, or the Nishigahara or CE(NiM95) strain (Fig. 3-5B).

These results indicate that the cell death induced by Ni-CE infection is associated with activation of executioner caspases.

PARP-1 cleavage is involved in M95-related cell death

Cleavage of PARP-1 by caspases is considered a hallmark of apoptosis (84). Thus, I investigated PARP-1 cleavage in SK-N-SH cells infected with each strain. Distinct PARP-1 cleavage was detected in cells infected with the Ni-CE and Ni(CEM95) strains and cells treated with Sts. However, PARP-1 cleavage was less pronounced in cells infected with the Nishigahara and CE(NiM95) strains than in those infected with the Ni-CE and Ni(CEM95) strains (Fig. 3-6). This result indicates that PARP-1 cleavage is involved in cell death induced by Ni-CE infection.

Cell death induced by Ni-CE infection is also related to the caspase-independent pathway

To investigate whether the cell death induced by Ni-CE infection depends on canonical caspase-dependent apoptosis, I investigated caspase-3/7 activity, PARP-1 cleavage, and cell viability of RABV-infected cells in the presence of the caspase inhibitor Z-VAD-FMK (Fig. 3-7). We demonstrated that Z-VAD-FMK significantly reduced

caspase-3/7 activity in SK-N-SH cells infected with the Ni-CE and Ni(CEM95) strains (Fig. 3-7A). Moreover, PARP-1 cleavage was partially recovered in cells infected with each RABV strain by treatment with Z-VAD-FMK (Fig. 3-7B). These results suggest that the mechanism of cell death induced by Ni-CE infection is related to executioner caspases in SK-N-SH cells. However, despite the fact that Z-VAD-FMK treatment at the same concentration inhibited the activity of caspase-3/7, there was no recovery of viable cells by Z-VAD-FMK treatment in cells infected with each virus strain (Fig. 3-7C). These results suggest that the cell death induced by Ni-CE infection depends on a caspase-independent pathway as well as caspase-dependent canonical apoptosis.

DISCUSSION

Previous studies have shown that attenuated RABV strains induce cell death both *in vitro* and *in vivo*, whereas virulent RABV strains showed less pronounced effects (11–13, 85). Therefore, the suppression of cell death induction is considered one of the mechanisms of RABV pathogenesis. However, the exact mechanism underlying cell death induced by attenuated RABV remains unknown. In this chapter, using the Nishigahara, Ni-CE, Ni(CEM95), and CE(NiM95) strains, I demonstrated that the amino acid at position 95 of the RABV-M protein plays a crucial role cell membrane disruption but not in PS exposure. Moreover, I showed that cell death induced by Ni-CE infection was not only associated with the caspase-3/7 pathway, the major executioner caspases in apoptosis, but also with the caspase-independent pathway.

When human SK-N-SH cells were inoculated with each RABV strain, the cells infected with the Ni-CE and Ni(95CEM) strains showed significant CPE and cell death and prominent DNA fragmentation, whereas those infected with the Nishigahara and CE(95NiM) strains induced low CPE or DNA fragmentation (Figs. 3-2 and 3-3). These results were similar to those from Mita *et al*. (41) in NA cells derived from mouse neuroblastomas. This suggests that the M95 mutation is involved in cell death in

neuroblastoma cells from different animal species.

A recent study has also shown that the RABV-M protein is a cytopathic determinant and that the amino acids at positions 67–79 of the M protein of the CVS-11 strain, a fixed RABV strain, are related to cell death characterized by DNA fragmentation, PARP-1 cleavage, and caspase-3 activation in mouse neuroblastoma N2a cells (83). Here, I found that the Ni-CE strain also induced DNA fragmentation, PARP-1 cleavage, and caspase-3/7 activation similar to that induced by the CVS-11 strain in human neuroblastoma SK-N-SH cells. Notably, it has been shown that the CVS-11 strain also activates both caspase-dependent and caspase-independent cell death pathways (85). These findings suggest that RABV-induced cell death may be caused by a common mechanism among multiple strains, although there are differences in the amino acid regions that determine it.

Although all strains used in this study induced PS exposure on the cell membrane, the Ni-CE and Ni(CEM95) strains, but not the Nishigahara and CE(NiM95) strains, dramatically induced cell membrane disruption (Fig. 3-4), strongly suggesting that M95 is related to cell membrane disruption. Thus, the M protein with Ala at M95 may induce cell membrane disruption followed by PS exposure, whereas the M protein with Val at M95 does not induce cell membrane disruption despite the occurrence of PS exposure (Fig. 3-8). Generally, cell membrane disruption occurs after PS exposure (86). Three

major mechanisms of PS exposure have been described thus far: (1) Ca^{2+}-mediated activation of TMEM16F; (2) caspase-mediated activation of Xkr8; and (3) caspase-mediated inactivation of the "flippase" complex, ATP11c and CDC50(87–90). In this study, I showed that cell death induced by Ni-CE infection was caspase-dependent in SK-N-SH cells, suggesting the involvement of either the Xkr8 or "flippase" complex mechanism. However, I found that SK-N-SH cells infected with the Ni-CE and Ni(CEM95) strains induced cell membrane disruption followed by PS exposure in the presence of Z-VAD-FMK (data not shown). Therefore, Ca^{2+}-mediated activation of TMEM16F, which is known as a caspase-independent phenomenon, may be associated with the M95-related cell death mechanism. Additionally, galectin-1, a β-galactoside-binding lectin, has been reported to induce PS exposure in neutrophils without altering cell viability (91). Therefore, the Ni-CE and Ni(CEM95) strains may also induce PS exposure by activating galectin-1. Further molecular studies are needed to elucidate the mechanism of cell death following PS exposure involving M95.

In this chapter, I showed that the PARP-1 cleavage during M95-related cell death was partially recovered by the caspase inhibitor, Z-VAD-FMK. PARP-1 is an intracellular protein that detects and repairs DNA breaks (92) and is mostly cleaved by activated caspase-3/7 (93, 94). However, PARP-1 cleavage is triggered by both caspase-dependent

and -independent pathways. Masdehors *et al*. (95) reported that PARP-1 cleavage may be regulated by a ubiquitin-associated "N-end rule pathway" in a caspase-independent manner. In contrast, Yang *et al*. (96) demonstrated that transforming growth factor-β, a cytokine involved in various physiological processes, induces PARP-1 cleavage in the presence of a caspase inhibitor. Thus, PARP-1 cleavage occurring during Ni-CE infection induced cell death may be associated with both caspase-dependent and caspase-independent signaling.

Here, we demonstrated that the Ni-CE strain induced cell death regardless of the presence of Z-VAD-FMK. Thus, caspase-independent programmed cell death mechanisms may also be associated with cell death induced by Ni-CE infection. New types of programmed cell death have been recently discovered (33), some of which are caspase-independent and induce antiviral immune responses (32, 97, 98). For instance, the M protein of the vesicular stomatitis virus (VSV), a member of the Rhabdoviridae family, is involved in novel cell death systems necroptosis and parthanatos (98, 99). Necroptosis is a newly discovered type of programmed cell death that is morphologically necrotic and caspase-independent. Receptor-interacting serine/threonine-protein 1 (RIPK1), a key signaling molecule in necroptosis (33), is upregulated in cells transfected with the VSV M protein (98). In contrast, the VSV M protein may also induce parthanatos,

which is another programmed cell death pathway that causes DNA fragmentation by PARP hyperactivation and apoptosis inducing factor activation (99, 100). I have not found any homologous amino acid regions between the VSV- and RABV-M proteins that might be associated with these novel forms of cell death. However, the question of whether the RABV-M protein activates these systems requires further investigation.

In the previous chapters, I described that M95 plays the critical role in SG formation. SGs generally inhibit apoptosis by suppressing the activation of apoptosis factors or the production of reactive oxygen species (101, 102). Thus, viruses with superior ability to induce SG formation can be expected to efficiently avoid apoptosis induction. However, previous studies demonstrated that the mutation at M95 from Val to Ala is responsible for programmed cell death including apoptosis; the Nishigahara and CE(NiM95) strains do not induce apoptosis, whereas Ni-CE and Ni(CEM95) strains do (41). A similar phenomenon illustrating this discrepancy has been reported for other viruses. For example, JEV induces dramatic apoptosis even though it also induces SGs, suggesting that JEV's apoptosis-inducing ability is so strong that it outweighs any ability to inhibit apoptosis through SG formation (9). Interestingly, the SG-constituent proteins TIA-1 and TIAR promote apoptosis in virus-infected cells, suggesting that SG factors switch from an anti-apoptotic response to an apoptotic response when SGs fail to degrade stressors and cells

become intolerant (25, 28, 103, 104). Thus, apoptosis of Ni-CE-infected cells may be the result of the apoptotic pathway more strongly than SG formation triggering the antiapoptotic pathway.

The mutation at M95 from Val to Ala plays an important role not only in SG formation and apoptosis, but also in pathogenesis: Ito *et al.* previously reported that the Ni-CE strain does not kill mice, but the CE(NiM95) strain does (39). In addition, I found that the Ni(CEM) strain is less pathogenic in mice than the Nishigahara strain, suggesting that SG formation by the Ni-CE strain may be related to RABV pathogenesis (data not shown). Since the Ni-CE and Ni(CEM95) strains induced RIG-I accumulation and IFN-β transcription more strongly than did the CE(NiM95) and Nishigahara strains, respectively (Fig. 2-4B), the pathogenesis involving M95 may be explained by innate immune evasion arising from the inhibition of the ability to induce SG formation. On the other hand, as mentioned above, the mutation at M95 from Val to Ala also affects the ability to induce cell death (41); this avoidance of cell death inhibits immune system activity and is a characteristic of RABV pathogenesis (11, 52, 53), and thus may also be involved in the pathogenesis of the virus. Further studies are needed to elucidate the mechanism in more detail *in vivo*.

In summary, I found that cell death induced by Ni-CE infection is characterized by

PS exposure following cell membrane disruption and is related to both of caspase-dependent and caspase-independent pathways in SK-N-SH cells (Fig. 3-8). Although the mechanisms by which a single amino acid change of M95 is involved in cell death remains unclear and the details of caspase-dependent and caspase-independent signaling are still unknown, there is high possibility that the cell death induced by Ni-CE infection involved in SGs, which results in the difference of pathogenesis between Nishigahara and Ni-CE strains.

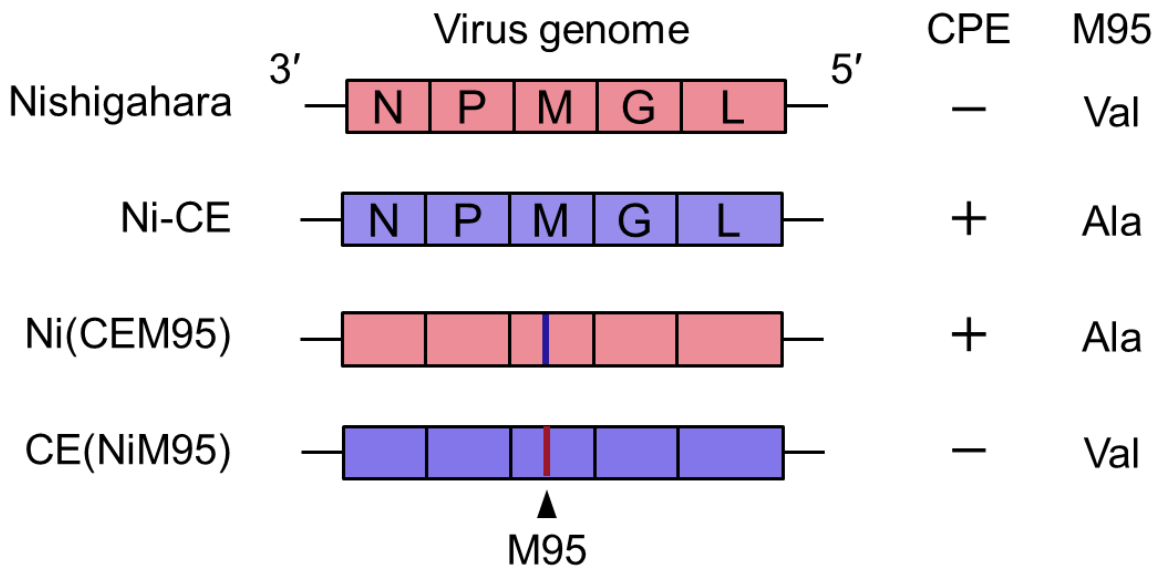

Fig. 3-1. Schematic diagram of the genome organization and CPE-inducing ability of the Nishigahara, Ni-CE, and M95-mutated strains in NA cells. Red and blue lines represent M95 derived from the Nishigahara (Val) or the Ni-CE strain (Ala), respectively. –, low CPE in NA cells; +, high CPE in NA cells (Mita *et al*., 2008).

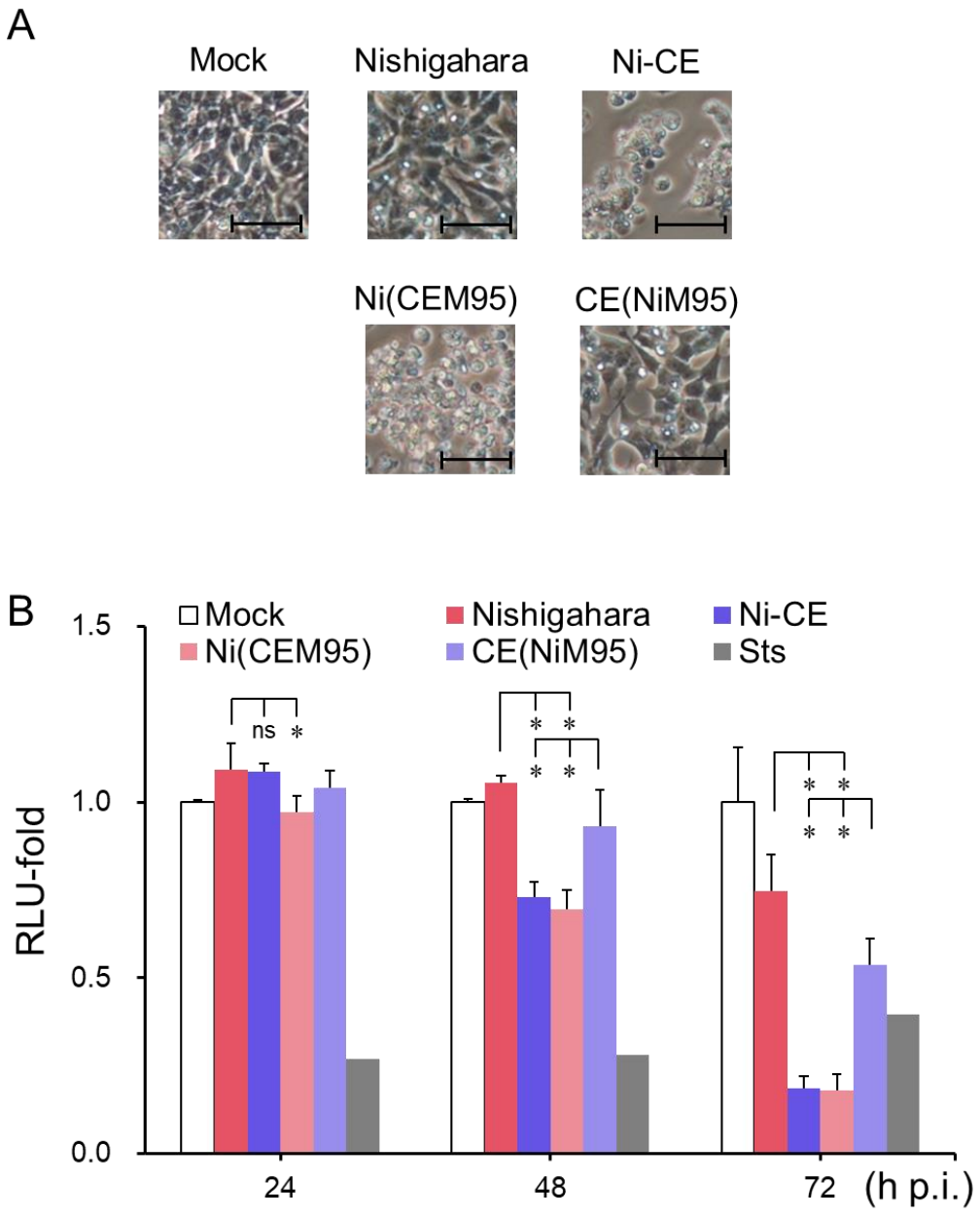

Fig. 3-2. Cell death induction by the Nishigahara, Ni-CE, and M95-mutated strains in human neuroblastoma SK-N-SH cells. (A) CPE induction by the Nishigahara, Ni-CE, and M95-mutated strains in SK-N-SH cells. Cells were infected with each strain (MOI of 1) and observed at 48 hpi with a microscope. Bars, 25 μm. (B) Viability of SK-N-SH cells infected with each strain at MOI of 3. After 24, 48, and 72 hpi, cell viability was measured using a Cell Titer Glo assay kit. Cells treated with 1.0 μM Sts for 4–6 h were used as positive controls. Luminescence is represented as the means and SD based on three wells; fold-changes in luminescence from the mock-infected sample are shown. Student–Newman–Keuls test was used to determine statistical significance. *, significant difference ($P < 0.05$).

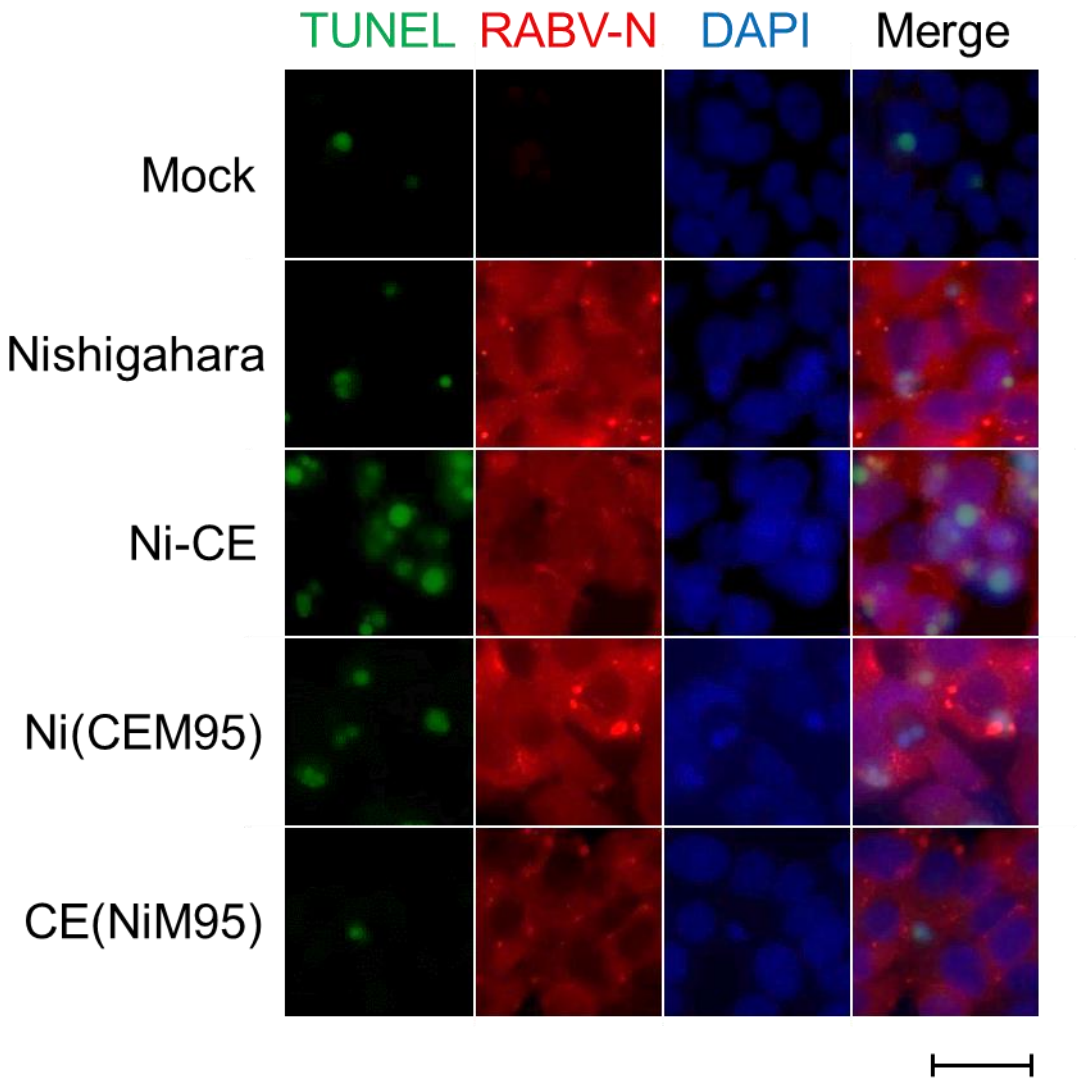

Fig. 3-3. Detection of apoptotic cells by TUNEL assay using SK-N-SH cells infected with the Nishigahara, Ni- CE, or M95- mutated strains. Cells were infected with each strain (MOI of 1). At 48 hpi, apoptotic cells were detected by TUNEL staining. Green staining shows apoptotic cells (TUNEL-positive). Red staining shows cells infected with RABV (targeting N protein). Blue staining shows cell nuclei (DAPI). Bar, 25 μm

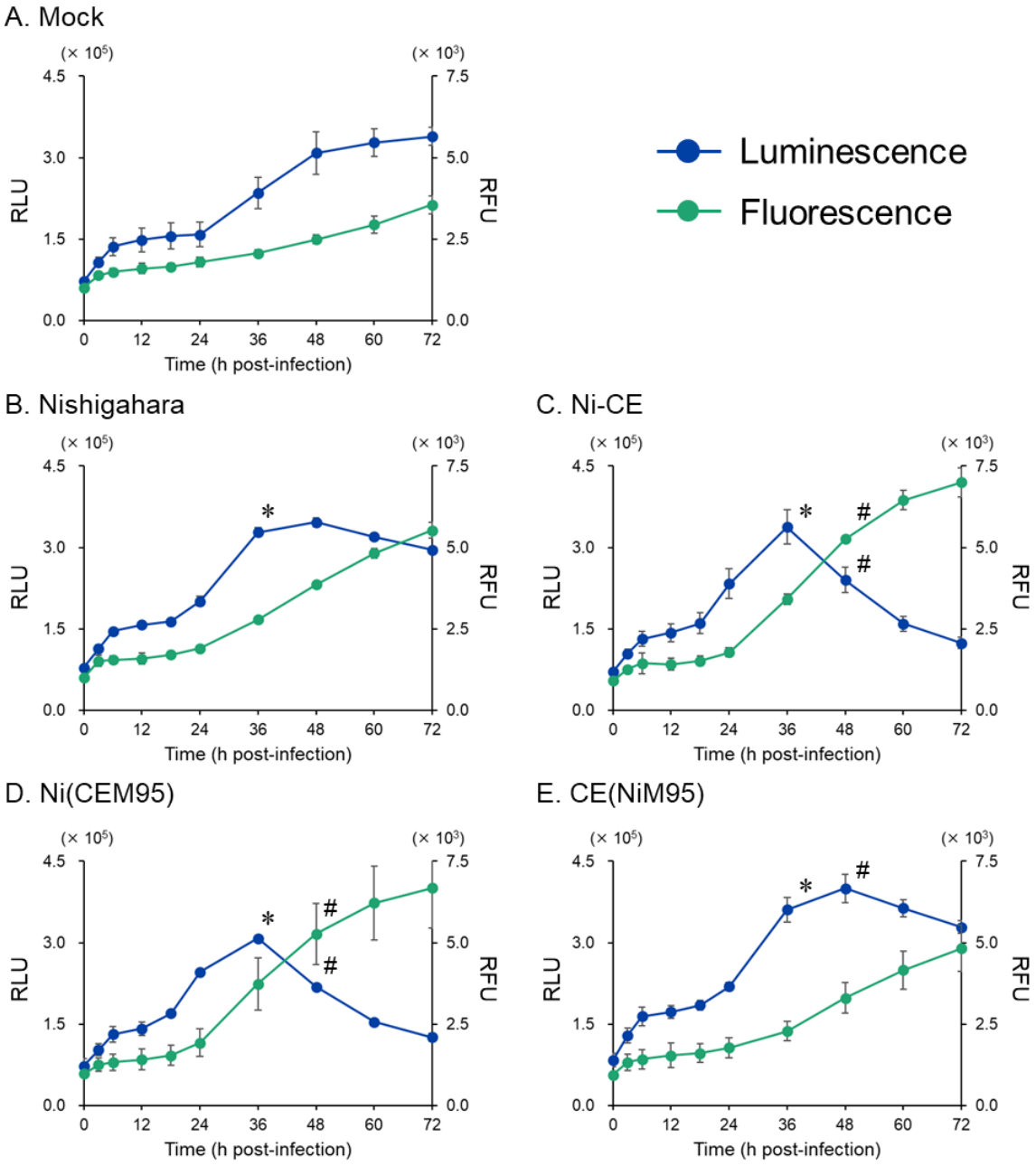

Fig. 3-4. Chronological analysis of PS exposure (luminescence) and cell membrane disruption (fluorescence). SK-N-SH cells were infected with mock (A) or the Nishigahara (B), Ni-CE (C), Ni(CEM95) (D), or CE(NiM95) (E) strain (MOI of 3). Luminescence and fluorescence are represented as the means and SD based on three wells. The Student–Newman–Keuls test was used to determine statistical significance. *, $P < 0.05$ compared with mock-infected cells; #, $P < 0.05$ compared with Nishigahara-infected cells.

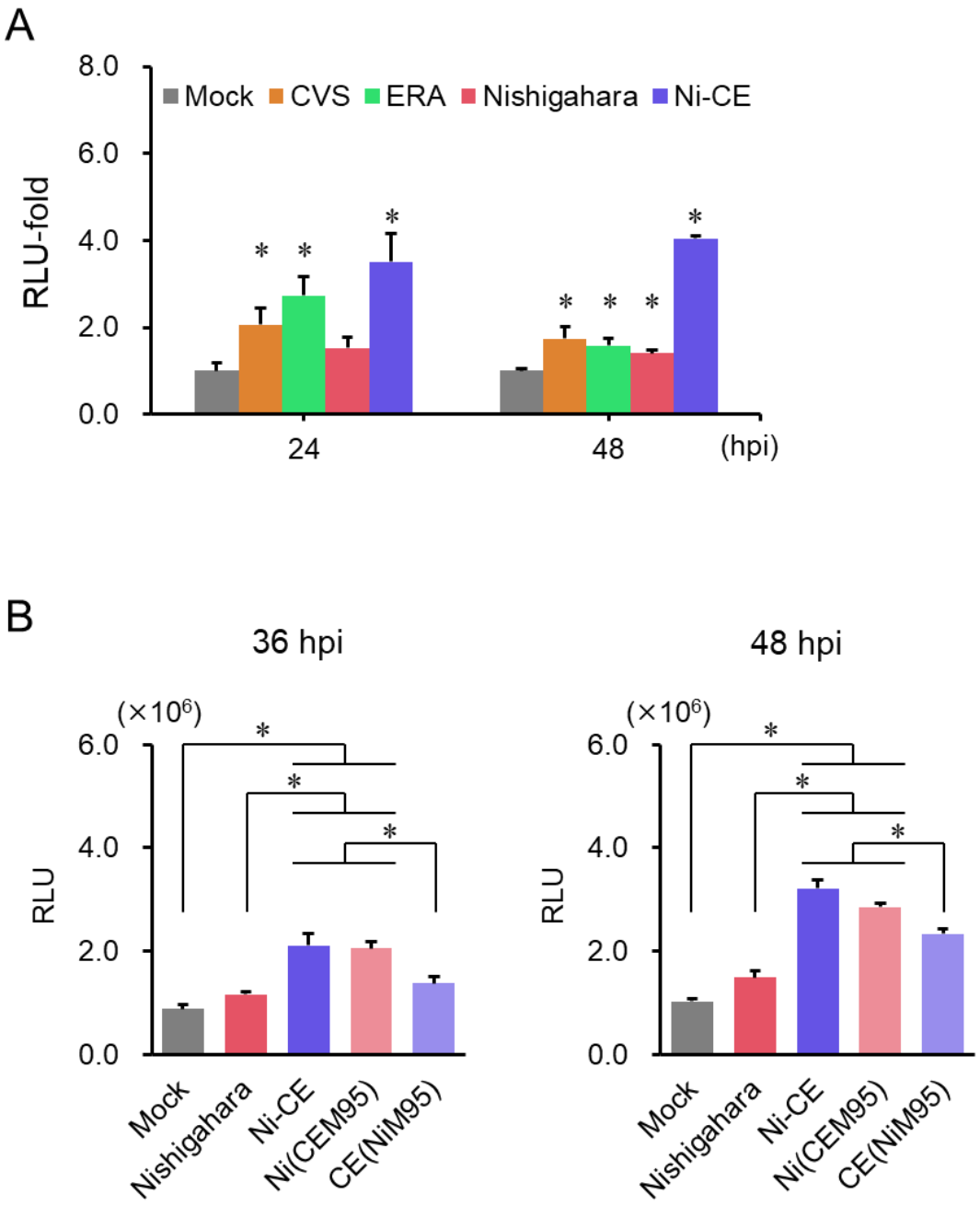

Fig. 3-5. Caspase-3/7 activities in RABV-infected SK-N-SH cells. (A) Caspase-3/7 activities in SK-N-SH cells infected with the CVS, ERA, Nishigahara, and Ni-CE strains (MOI of 1) at 24 hpi and 48 hpi. Fold-changes in luminescence from the mock-infected sample are shown. The Student–Newman–Keuls test was used to determine statistical significance. *, Significant difference versus mock-infected cells ($P < 0.05$). (B) Caspase-3/7 activities in SK-N-SH cells infected with the Nishigahara, Ni-CE, Ni(CEM95) and CE(NiM95) strains at 36 and 48 hpi. Luminescence is represented by the means and SD based on three wells. The Student–Newman–Keuls test was used to determine statistical significance. *, $P < 0.05$.

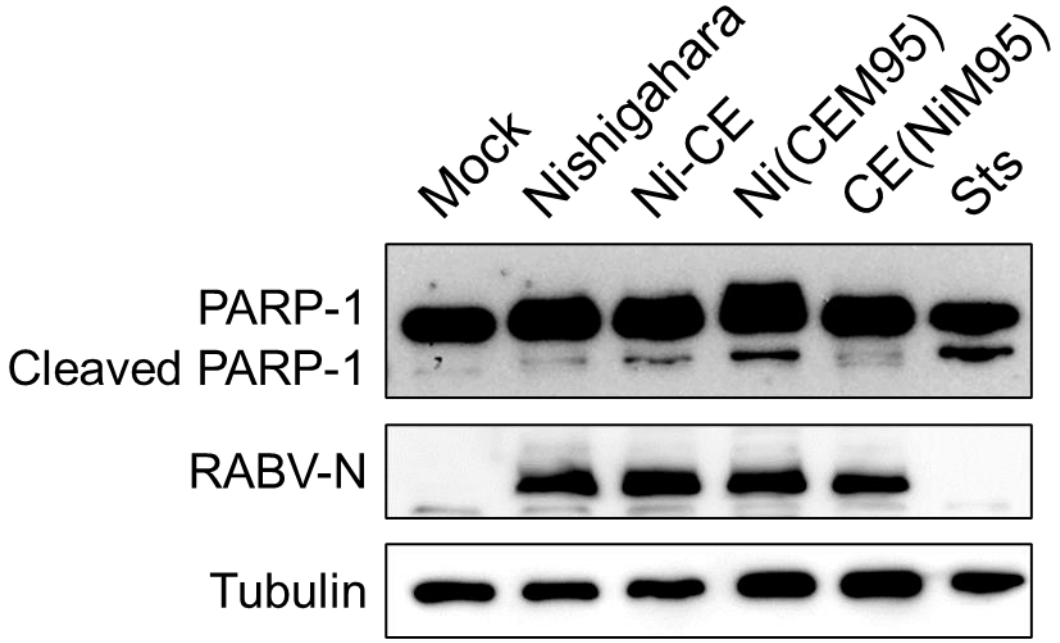

Fig. 3-6. Western blot analysis of PARP-1 cleavage. SK-N-SH cells were infected with each RABV strain (MOI of 1) and lysed at 24 hpi. Cells treated with 1.0 μM Sts for 4–6 h were used as positive controls. Proteins were detected with antibodies against PARP-1 and RABV-N. Tubulin was used as a loading control.

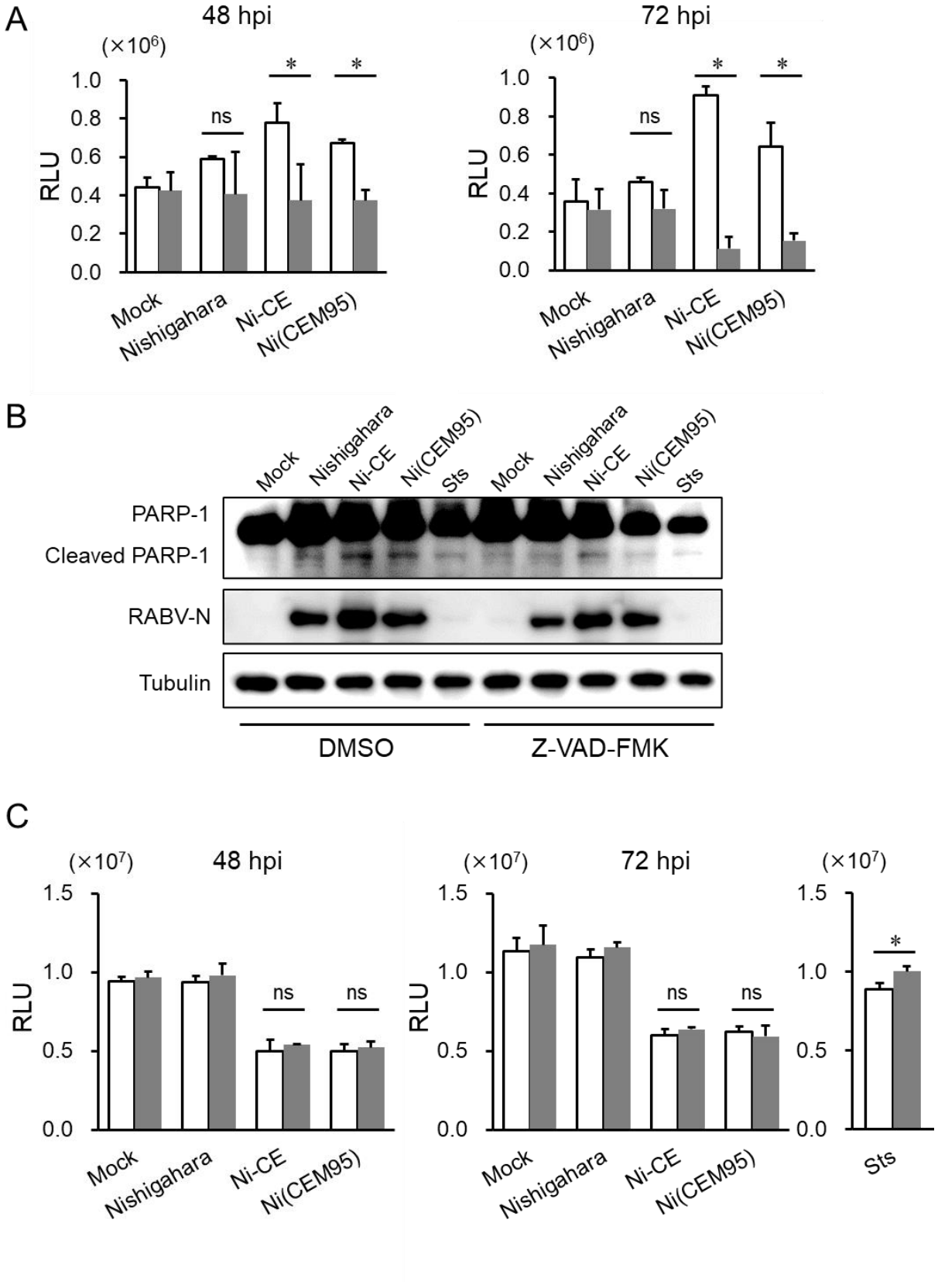
A
48 hpi
72 hpi
(×10^6)
RLU
1.0
0.8
0.6
0.4
0.2
0.0
ns
*
Mock
Nishigahara
Ni-CE
Ni(CEM95)
B
Mock
Nishigahara
Ni-CE
Ni(CEM95)
Sts
PARP-1
Cleaved PARP-1
RABV-N
Tubulin
DMSO
Z-VAD-FMK
C
(×10^7)
48 hpi
72 hpi
1.5
1.0
0.5
0.0
Sts

Fig. 3-7. Effect of the caspase inhibitor Z-VAD-FMK on caspase-3/7 activity, cell viability, and PARP-1 cleavage on SK-N-SH cells infected with the Nishigahara, Ni-CE, and Ni(CEM95) strains. (A) Effects of the caspase inhibitor Z-VAD-FMK on caspase-3/7 activity in SK-N-SH cells infected with the Nishigahara, Ni-CE, and Ni(CEM95) strains (MOI of 1). DMSO (white bars) or Z-VAD-FMK (20 μM: grey bars) was treated after RABV infection. After 48 and 72 hpi, Caspase-3/7 activity was measured. Luminescence is represented as the means and SD based on three wells. The Student–Newman–Keuls test was used to determine statistical significance. *, significant difference ($P < 0.05$). (B) SK-N-SH cells were infected with each RABV strain (MOI of 1). Cells were treated with DMSO or Z-VAD-FMK (20 μM) after RABV infection and lysed at 48 hpi. Cells treated with 1.0 μM Sts for 4–6 h were used as positive controls. Proteins were detected with antibodies against PARP-1 and RABV-N. Tubulin was used as a loading control. (C) Effect of Z-VAD-FMK treatment on the viability of SK-N-SH cells infected with each RABV strain (MOI of 1). Cells were treated with DMSO (white bars) or Z-VAD-FMK (20 μM: grey bars) after RABV infection. At 48 hpi and 72 hpi, cell viability was measured using a Cell Titer Glo assay kit. Cells treated with 0.1 μM Sts for 72 h were used as positive controls. Luminescence is represented as the means and SD based on three wells. The Student–Newman–Keuls test was used to determine statistical significance. *, significant difference ($P < 0.05$).

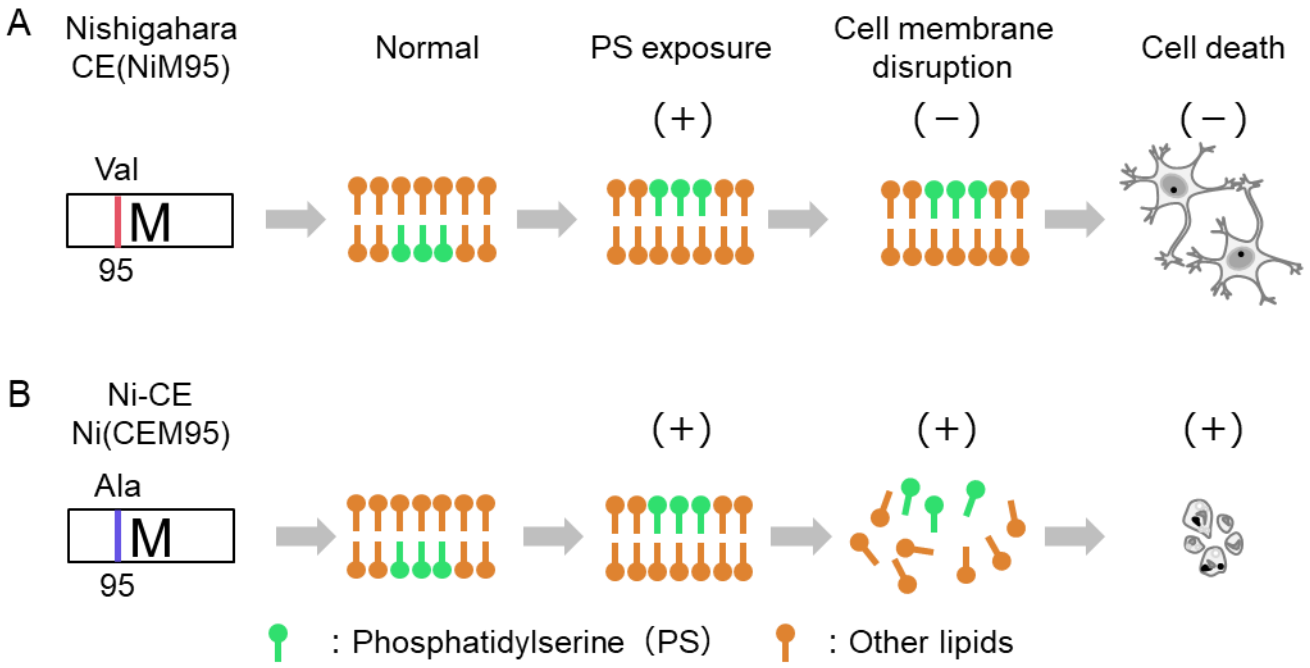

Fig. 3-8. Summary of M95-related cell membrane dynamics in SK-N-SH cells infected with RABV.

(A) The Nishigahara or CE(NiM95) strain does not induce cell membrane disruption despite PS exposure.

(B) The Ni-CE or Ni(CEM95) strain induces cell membrane disruption through PS exposure.

Concluding Remarks

RABV causes neurological disease in mammals including humans, resulting in approximately 59,000 human deaths occurring annually worldwide. Although the molecular mechanisms of RABV pathogenesis and evasion of host immune response need to be elucidated to develop effective therapies after disease onset, much remained unknown about these mechanisms. To elucidate part of the pathogenic mechanism, I focused on the relationship between SGs and RABV, and I have demonstrated that M95 plays a critical role in SG formation and programmed cell death.

In chapter I, I revealed that the virulent fixed Nishigahara strain inhibits SG formation, whereas the Ni-CE strain, a non-lethal offshoot of the Nishigahara strain, does not. Furthermore, I identified that M95 plays a critical role in SG formation; M95 at Val plays a role in inhibiting SG formation and programmed cell death, whereas M95 at Ala does not.

In chapter II, I demonstrated that RIG-I utilizes M95-related SGs, which are formed by PKR-activation and eIF2α-phosphorylation as a scaffold to recognize the RABV genome, promoting IFN-β transcription.

In chapter III, I described a further investigation of unknown aspects of the

mechanism related to M95, conducted because M95 was previously reported to involve in programmed cell death and RABV pathogenesis, and demonstrated the involvement of apoptosis and a new type of programmed cell death.

To conclude, I have demonstrated that M95 plays a critical role in SG formation and programmed cell death. These results suggest that Ni-CE-infected cells form SGs to inhibit viral replication, and programmed cell death is induced when this formation fails. I believe that elucidation of these mechanisms represents a major step forward in the understanding of RABV pathogenesis and in the knowledge required for future therapeutic development.

Acknowledgement

First, I am forever indebted to my supervisor, Dr. Tatsunori Masatani (Associate Professor in the Laboratory of Zoonotic Diseases, Faculty of Applied Biological Sciences, Gifu University) for his dedicated supervision and inspirational guidance over the last four years.

I would like to express my sincere appreciation to another supervisor, Dr. Makoto Ozawa (Associate Professor in Laboratory of Animal Hygiene, Joint Faculty of Veterinary Medicine, Kagoshima University) for his valuable advice, stimulating ideas, and technical input.

I am also grateful to Dr. Kosuke Okuya (Assistant Professor in the Transboundary Animal Disease Research Center, Joint Faculty of Veterinary Medicine, Kagoshima University) for his technical guidance.

I am also particularly grateful to Dr. Yoshikazu Fujimoto (Associate Professor in the Transboundary Animal Disease Research Center, Joint Faculty of Veterinary Medicine,

Kagoshima University) and Dr. Ken Maeda (Professor in the Joint Faculty of Veterinary Medicine, Yamaguchi University) for their guidance as co-supervisors.

I would also like to express my gratitude to Dr. Hiroshi Shimoda (Assistant Professor in the Laboratory of Veterinary Microbiology, Joint Faculty of Veterinary Medicine, Yamaguchi University), Dr. Takehisa Chuma (Professor in the Laboratory of Veterinary Public Health, Joint Faculty of Veterinary Medicine, Kagoshima University), Dr. Tetsuya Tanaka (Professor in the Laboratory of Infectious Diseases, Joint Faculty of Veterinary Medicine, Kagoshima University), Dr. Kyoko Tsukiyama-Kohara (Professor in the Transboundary Animal Diseases Research Center, Joint Faculty of Veterinary Medicine, Kagoshima University), and Dr. Mitsuya Shiraishi (Professor in the Department of Basic Veterinary Science, Joint Faculty of Veterinary Medicine, Kagoshima University) for their valuable advice and review of this thesis.

I am also particularly grateful to Editage (https://www. editage. jp/) and Mr. Henry Smith (Joint Graduate School of Veterinary Medicine, Kagoshima University) for their language assistance.

I sincerely thank Dr. Naoto Ito (Professor in the Laboratory of Zoonotic Diseases, Faculty of Applied Biological Sciences, Gifu University) and Dr. Makoto Sugiyama (Vice-President of Gifu University and Professor in the Faculty of Applied Biological Sciences, Gifu University) for their eminent help and valuable advice. I also wish to thank all members of the Laboratory of Zoonotic Diseases at Gifu University for their technical assistance.

I would like to thank Dr. Takemasa Sakaguchi (Professor in the Department of Virology, Graduate School of Biomedical Sciences, Hiroshima University), Dr. Kiyotada Naitou (Associate Professor in the Department of Basic Veterinary Science, Joint Faculty of Veterinary Medicine, Kagoshima University), Dr. Koji Onomoto (Assistant Professor in the Division of Molecular Immunology, Medical Mycology Research Center, Chiba University), Dr. Mitsutoshi Yoneyama (Professor in the Division of Molecular Immunology, Medical Mycology Research Center, Chiba University), and Dr. Takashi Fujita (Professor in the Division of Integrated Life Science, Graduate School of Biostudies, Kyoto University) for their technical input.

This study was supported partially by the Japan Society for the Promotion of Science (JSPS) Grant- Aid for Scientific Research (KAKENHI: grant no. 17K08083) and GSK Japan Research Grant 2020 for Tatsunori Masatani, and a grant-in-aid for JSPS Research Fellows (grant no. JP22J13293) to Isshu Kojima.

Finally, I would like to express my sincere gratitude to my fellow-lab members, friends, and my family, especially my parents, for their support throughout the doctoral program.

.

References

1. Knobel DL, Cleaveland S, Coleman PG, Fèvre EM, Meltzer MI *et al*. 2005. Re-evaluating the burden of rabies in Africa and Asia. Bull World Heal Organ 83:360–368.

2. Fisher CR, Schnell MJ. 2018. New developments in rabies vaccination. Rev Sci Tech l'OIE 37:657–672.

3. Willoughby RE, Tieves KS, Hoffman GM, Ghanayem NS, Amlie-Lefond CM *et al*. 2005. Survival after treatment of rabies with induction of coma. N Engl J Med 352:2508–2514.

4. Ledesma LA, Lemos ERS, Horta MA. 2020. Comparing clinical protocols for the treatment of human rabies: the Milwaukee protocol and the Brazilian protocol (Recife). Rev Soc Bras Med Trop 53:e20200352.

5. Jackson AC. 2016. Human rabies: a 2016 update. Curr Infect Dis Rep 18:1–6.

6. Mancini M, Vidal SM. 2018. Insights into the pathogenesis of herpes simplex encephalitis from mouse models. Mamm Genome 29:425–445.

7. Ashraf U, Ding Z, Deng S, Ye J, Cao S, Chen Z. 2021. Pathogenicity and virulence of Japanese encephalitis virus: Neuroinflammation and neuronal cell

damage. Virulence 12:968–980.

8. Chen C-J, Ou Y-C, Chang C-Y, Pan H-C, Liao S-L *et al*. 2012. Glutamate released by Japanese encephalitis virus-infected microglia involves TNF-α signaling and contributes to neuronal death. Glia 60:487–501.

9. Wang Q, Xin X, Wang T, Wan J, Ou Y *et al*. 2019. Japanese encephalitis virus induces apoptosis and encephalitis by activating the PERK pathway. J Virol 93.

10. Scott CA, Rossiter JP, Andrew RD, Jackson AC. 2008. Structural abnormalities in neurons are sufficient to explain the clinical disease and fatal outcome of experimental rabies in yellow fluorescent protein-expressing transgenic mice. J Virol 82:513–521.

11. Morimoto K, Hooper DC, Spitsin S, Koprowski H, Dietzschold B. 1999. Pathogenicity of different rabies virus variants inversely correlates with apoptosis and rabies virus glycoprotein expression in infected primary neuron cultures. J Virol 73:510–518.

12. Yan X, Prosniak M, Curtis MT, Weiss ML, Faber M *et al*. 2001. Silver-haired bat rabies virus variant does not induce apoptosis in the brain of experimentally infected mice. J Neurovirol 7:518–527.

13. Thoulouze MI, Lafage M, Montano-Hirose JA, Lafon M. 1997. Rabies virus

infects mouse and human lymphocytes and induces apoptosis. J Virol 71:7372–7380.

14. Chenik M, Chebli K, Gaudin Y, Blondel D. 1994. In vivo interaction of rabies virus phosphoprotein (P) and nucleoprotein (N): Existence of two N-binding sites on P protein. J Gen Virol 75:2889–2896.

15. Albertini AA V., Wernimont AK, Muziol T, Ravelli RBG, Clapier CR *et al*. 2006. Crystal structure of the rabies virus nucleoprotein-RNA complex. Science 313:360–363.

16. Wirblich C, Tan GS, Papaneri A, Godlewski PJ, Orenstein JM *et al*. 2008. PPEY motif within the rabies virus (RV) matrix protein is essential for efficient virion release and RV pathogenicity. J Virol 82:9730–9738.

17. Finke S, Conzelmann K-K. 2003. Dissociation of rabies virus matrix protein functions in regulation of viral RNA synthesis and virus assembly. J Virol 77:12074–12082.

18. Dietzschold B, Li J, Faber M, Schnell M. 2008. Concepts in the pathogenesis of rabies. Future Virol 3:481–490.

19. Finke S, Conzelmann K-K. 2005. Replication strategies of rabies virus. Virus Res 111:120–131.

20. Akira S, Uematsu S, Takeuchi O. 2006. Pathogen recognition and innate immunity. Cell 124:783–801.

21. Hossain MA, Larrous F, Rawlinson SM, Zhan J, Sethi A *et al*. 2019. Structural elucidation of viral antagonism of innate immunity at the STAT1 interface. Cell Rep 29:1934-1945.e8.

22. Randall RE, Goodbourn S. 2008. Interferons and viruses: An interplay between induction, signalling, antiviral responses and virus countermeasures. J Gen Virol 89:1–47.

23. Fujita T. 2006. Sensing Viral RNA Amid Your Own. Science 314:935–936.

24. Hofmann S, Kedersha N, Anderson P, Ivanov P. 2021. Molecular mechanisms of stress granule assembly and disassembly. Biochim Biophys Acta - Mol Cell Res 1868.

25. Eiermann N, Haneke K, Sun Z, Stoecklin G, Ruggieri A. 2020. Dance with the devil: Stress granules and signaling in antiviral responses. Viruses 12:1–47.

26. Onomoto K, Yoneyama M, Fung G, Kato H, Fujita T. 2014. Antiviral innate immunity and stress granule responses. Trends Immunol 35:420–428.

27. Mahboubi H, Stochaj U. 2017. Cytoplasmic stress granules: Dynamic modulators of cell signaling and disease. Biochim Biophys Acta - Mol Basis Dis 1863:884–

895.

28. Kedersha N, Ivanov P, Anderson P. 2013. Stress granules and cell signaling: more than just a passing phase? Trends Biochem Sci 38:494–506.

29. Hofmann S, Kedersha N, Anderson P, Ivanov P. 2021. Molecular mechanisms of stress granule assembly and disassembly. Biochim Biophys Acta - Mol Cell Res 1868:118876.

30. Onomoto K, Onoguchi K, Yoneyama M. 2021. Regulation of RIG-I-like receptor-mediated signaling: interaction between host and viral factors. Cell Mol Immunol 18:539–555.

31. Yoneyama M, Onomoto K, Jogi M, Akaboshi T, Fujita T. 2015. Viral RNA detection by RIG-I-like receptors. Curr Opin Immunol 32:48–53.

32. Tang D, Kang R, Berghe T Vanden, Vandenabeele P, Kroemer G. 2019. The molecular machinery of regulated cell death. Cell Res 29:347–364.

33. Galluzzi L, Vitale I, Aaronson SA, Abrams JM, Adam D *et al*. 2018. Molecular mechanisms of cell death: Recommendations of the nomenclature committee on cell death 2018. Cell Death Differ 25:486–541.

34. Schaefer J, Clow W, Bhandari R, Kimura M, Williams L, Pellegrini M. 2022. Killing in self-defense: proapoptotic drugs to eliminate intracellular pathogens.

Curr Opin Immunol 79:102263.

35. Zan J, Liu J, Zhou J-W, Wang H-L, Mo K-K *et al*. 2016. Rabies virus matrix protein induces apoptosis by targeting mitochondria. Exp Cell Res 347:83–94.

36. Christophe P, Stephanie L, Bernhard D, Monique L. 2003. Glycoprotein of nonpathogenic rabies viruses is a key determinant of human cell apoptosis. J Virol 77:10537–10547.

37. Kassis R, Larrous F, Estaquier J, Bourhy H. 2004. Lyssavirus matrix protein induces apoptosis by a TRAIL-dependent mechanism involving caspase-8 activation. J Virol 78:6543–6555.

38. Masatani T, Ito N, Shimizu K, Ito Y, Nakagawa K *et al*. 2011. Amino acids at positions 273 and 394 in rabies virus nucleoprotein are important for both evasion of host RIG-I-mediated antiviral response and pathogenicity. Virus Res 155:168–174.

39. Ito N, Mita T, Shimizu K, Ito Y, Masatani T *et al*. 2011. Amino acid substitution at position 95 in rabies virus matrix protein affects viral pathogenicity. J Vet Med Sci 73:1363–1366.

40. Shimizu K, Ito N, Mita T, Yamada K, Hosokawa-Muto J *et al*. 2007. Involvement of nucleoprotein, phosphoprotein, and matrix protein genes of rabies

virus in virulence for adult mice. Virus Res 123:154–160.

41. Mita T, Shimizu K, Ito N, Yamada K, Ito Y *et al*. 2008. Amino acid at position 95 of the matrix protein is a cytopathic determinant of rabies virus. Virus Res 137:33–39.

42. Guzikowski AR, Chen YS, Zid BM. 2019. Stress-induced mRNP granules: Form and function of processing bodies and stress granules. Wiley Interdiscip Rev RNA 10:1–17.

43. Moser JJ, Fritzler MJ. 2010. Cytoplasmic ribonucleoprotein (RNP) bodies and their relationship to GW/P bodies. Int J Biochem Cell Biol 42:828–843.

44. Tourrière H, Chebli K, Zekri L, Courselaud B, Blanchard JM *et al*. 2003. The RasGAP-associated endoribonuclease G3BP assembles stress granules. J Cell Biol 160:823–831.

45. Kedersha N, Chen S, Gilks N, Li W, Miller IJ *et al*. 2002. Evidence that ternary complex (eIF2-GTP-tRNA i Met)–deficient preinitiation complexes are core constituents of mammalian stress granules. Mol Biol Cell 13:195–210.

46. Nikolic J, Civas A, Lama Z, Lagaudrière-Gesbert C, Blondel D. 2016. Rabies virus infection induces the formation of stress granules closely connected to the viral factories. PLOS Pathog 12:e1005942.

47. Yamada K, Ito N, Takayama-Ito M, Sugiyama M, Minamoto N. 2006. Multigenic relation to the attenuation of rabies virus. Microbiol Immunol 50:25–32.

48. Takahashi T, Inukai M, Sasaki M, Potratz M, Jarusombuti S *et al*. 2020. Genetic and phenotypic characterization of a rabies virus strain isolated from a dog in Tokyo, Japan in the 1940s. Viruses 12:914.

49. Yamada K, Park C-H, Noguchi K, Kojima D, Kubo T *et al*. 2012. Serial passage of a street rabies virus in mouse neuroblastoma cells resulted in attenuation: Potential role of the additional N-glycosylation of a viral glycoprotein in the reduced pathogenicity of street rabies virus. Virus Res 165:34–45.

50. Isomura M, Yamada K, Noguchi K, Nishizono A. 2017. Near-infrared fluorescent protein iRFP720 is optimal for in vivo fluorescence imaging of rabies virus infection. J Gen Virol 98:2689–2698.

51. Minamoto N, Tanaka H, Hishida M, Goto H, Ito H *et al*. 1994. Linear and conformation-dependent antigenic sites on the nucleoprotein of rabies virus. Microbiol Immunol 38:449–455.

52. Jackson AC, Rasalingam P, Weli SC. 2006. Comparative pathogenesis of recombinant rabies vaccine strain SAD-L16 and SAD-D29 with replacement of

Arg333 in the glycoprotein after peripheral inoculation of neonatal mice: Less neurovirulent strain is a stronger inducer of neuronal apoptosis. Acta Neuropathol 111:372–378.

53. Suja MS, Mahadevan A, Madhusudana SN, Shankar SK. 2011. Role of apoptosis in rabies viral encephalitis: A comparative study in mice, canine, and human brain with a review of literature. Patholog Res Int 2011:1–13.

54. Kedersha NL, Gupta M, Li W, Miller I, Anderson P. 1999. RNA-binding proteins TIA-1 and TIAR link the phosphorylation of eIF-2α to the assembly of mammalian stress granules. J Cell Biol 147:1431–1442.

55. Pakos-Zebrucka K, Koryga I, Mnich K, Ljujic M, Samali A, Gorman AM. 2016. The integrated stress response. EMBO Rep 17:1374–1395.

56. Gale M, Katze MG. 1998. Molecular mechanisms of interferon resistance mediated by viral-directed inhibition of PKR, the interferon-induced protein kinase. Pharmacol Ther 78:29–46.

57. Reineke LC, Lloyd RE. 2015. The stress granule protein G3BP1 recruits protein kinase R to promote multiple innate immune antiviral responses. J Virol 89:2575–2589.

58. Yang W, Ru Y, Ren J, Bai J, Wei J *et al*. 2019. G3BP1 inhibits RNA virus

replication by positively regulating RIG-I-mediated cellular antiviral response. Cell Death Dis 10:946.

59. Yoo J-S, Takahasi K, Ng CS, Ouda R, Onomoto K *et al*. 2014. DHX36 enhances RIG-I signaling by facilitating PKR-mediated antiviral stress granule formation. PLoS Pathog 10:e1004012.

60. Onomoto K, Jogi M, Yoo J-S, Narita R, Morimoto S *et al*. 2012. Critical role of an antiviral stress granule containing RIG-I and PKR in viral detection and innate immunity. PLoS One 7:e43031.

61. Yoneyama M, Jogi M, Onomoto K. 2016. Regulation of antiviral innate immune signaling by stress-induced RNA granules. J Biochem 159:279–286.

62. Mok BW-Y, Song W, Wang P, Tai H, Chen Y *et al*. 2012. The NS1 protein of influenza A virus interacts with cellular processing bodies and stress granules through RNA-associated protein 55 (RAP55) during virus infection. J Virol 86:12695–12707.

63. Khaperskyy DA, Hatchette TF, McCormick C. 2012. Influenza A virus inhibits cytoplasmic stress granule formation. FASEB J 26:1629–1639.

64. Nelson E V., Schmidt KM, Deflubé LR, Doğanay S, Banadyga L *et al*. 2016. Ebola virus does not induce stress granule formation during infection and

sequesters stress granule proteins within viral inclusions. J Virol 90:7268–7284.

65. Le Sage V, Cinti A, McCarthy S, Amorim R, Rao S *et al*. 2017. Ebola virus VP35 blocks stress granule assembly. Virology 502:73–83.

66. Kobasa D, Rodgers ME, Wells K, Kawaoka Y. 1997. Neuraminidase hemadsorption activity, conserved in avian influenza A viruses, does not influence viral replication in ducks. J Virol 71:6706–6713.

67. Reineke LC, Dougherty JD, Pierre P, Lloyd RE. 2012. Large G3BP-induced granules trigger eIF2α phosphorylation. Mol Biol Cell 23:3499–3510.

68. Yoshida A, Kawabata R, Honda T, Tomonaga K, Sakaguchi T, Irie T. 2015. IFN-β-inducing, unusual viral RNA species produced by paramyxovirus infection accumulated into distinct cytoplasmic structures in an RNA-type-dependent manner. Front Microbiol 6:1–13.

69. Kim SS-Y, Sze L, Lam K. 2019. The stress granule protein G3BP1 binds viral dsRNA and RIG-I to enhance interferon-β response. J Biol Chem 294:6430–6438.

70. Schoggins JW, Rice CM. 2011. Interferon-stimulated genes and their antiviral effector functions. Curr Opin Virol 1:519–525.

71. Toroney R, Nallagatla SR, Boyer JA, Cameron CE, Bevilacqua PC. 2010.

Regulation of PKR by HCV IRES RNA: Importance of domain II and NS5A. J Mol Biol 400:393–412.

72. Yue Z, Shatkin AJ. 1997. Double-stranded RNA-dependent protein kinase (PKR) is regulated by reovirus structural proteins. Virology 234:364–371.

73. Davies M V, Chang HW, Jacobs BL, Kaufman RJ. 1993. The E3L and K3L vaccinia virus gene products stimulate translation through inhibition of the double-stranded RNA-dependent protein kinase by different mechanisms. J Virol 67:1688–1692.

74. Barber MRW, Aldridge JR, Webster RG, Magor KE. 2010. Association of RIG-I with innate immunity of ducks to influenza. Proc Natl Acad Sci 107:5913–5918.

75. Visser LJ, Medina GN, Rabouw HH, de Groot RJ, Langereis MA *et al*. 2019. Foot-and-mouth disease virus leader protease cleaves G3BP1 and G3BP2 and inhibits stress granule formation. J Virol 93.

76. Nakagawa K, Narayanan K, Wada M, Makino S. 2018. Inhibition of stress granule formation by middle sast respiratory syndrome coronavirus 4a accessory protein facilitates viral translation, leading to efficient virus replication. J Virol 92:1–19.

77. Rabouw HH, Langereis MA, Knaap RCM, Dalebout TJ, Canton J *et al*. 2016.

Middle east respiratory coronavirus accessory protein 4a inhibits PKR-mediated antiviral stress responses. PLOS Pathog 12:e1005982.

78. Li T, Li X, Zhu W, Wang H, Mei L *et al*. 2016. NF90 is a novel influenza A virus NS1-interacting protein that antagonizes the inhibitory role of NS1 on PKR phosphorylation. FEBS Lett 590:2797–2810.

79. Ashkenazi A, Dixit VM. 1998. Death receptors: Signaling and modulation. Science 281:1305–1308.

80. Julien O, Wells JA. 2017. Caspases and their substrates. Cell Death Differ 24:1380–1389.

81. Larsen BD, Sørensen CS. 2017. The caspase-activated DNase: Apoptosis and beyond. FEBS J 284:1160–1170.

82. Suzuki J, Imanishi E, Nagata S. 2016. Xkr8 phospholipid scrambling complex in apoptotic phosphatidylserine exposure. Proc Natl Acad Sci 113:9509–9514.

83. Zan J, Liu J, Zhou JW, Wang HL, Mo KK *et al*. 2016. Rabies virus matrix protein induces apoptosis by targeting mitochondria. Exp Cell Res 347:83–94.

84. Chaitanya GV, Alexander JS, Babu PP. 2010. PARP-1 cleavage fragments: Signatures of cell-death proteases in neurodegeneration. Cell Commun Signal 8:1–11.

85. Sarmento L, Tseggai T, Dhingra V, Fu ZF. 2006. Rabies virus-induced apoptosis involves caspase-dependent and caspase-independent pathways. Virus Res 121:144–151.

86. Silva MT, do Vale A, dos Santos NMN. 2008. Secondary necrosis in multicellular animals: An outcome of apoptosis with pathogenic implications. Apoptosis 13:463–482.

87. Segawa K, Kurata S, Yanagihashi Y, Brummelkamp TR, Matsuda F, Nagata S. 2014. Caspase-mediated cleavage of phospholipid flippase for apoptotic phosphatidylserine exposure. Science 344:1164–1168.

88. Suzuki J, Umeda M, Sims PJ, Nagata S. 2010. Calcium-dependent phospholipid scrambling by TMEM16F. Nature 468:834–838.

89. Suzuki J, Denning DP, Imanishi E, Horvitz HR, Nagata S. 2013. Xk-related protein 8 and CED-8 promote phosphatidylserine exposure in apoptotic cells. Science 341:403–406.

90. Suzuki J, Fujii T, Imao T, Ishihara K, Kuba H, Nagata S. 2013. Calcium-dependent phospholipid scramblase activity of TMEM16 protein family members. J Biol Chem 288:13305–13316.

91. Stowell SR, Karmakar S, Arthur CM, Ju T, Rodrigues LC *et al*. 2009. Galectin-1

induces reversible phosphatidylserine exposure at the plasma membrane. Mol Biol Cell 20:1408–1418.

92. Ivana Scovassi A, Diederich M. 2004. Modulation of poly(ADP-ribosylation) in apoptotic cells. Biochem Pharmacol 68:1041–1047.

93. Salvesen GS, Dixit VM. 1997. Caspases: Intracellular signaling by proteolysis. Cell 91:443–446.

94. Boucher D, Blais V, Denault JB. 2012. Caspase-7 uses an exosite to promote poly(ADP ribose) polymerase 1 proteolysis. Proc Natl Acad Sci U S A 109:5669–5674.

95. Masdehors P, Glaisner S, Maciorowski Z, Magdelénat H, Delic J. 2000. Ubiquitin-dependent protein processing controls radiation-induced apoptosis through the N-end rule pathway. Exp Cell Res 257:48–57.

96. Tian Q, Wang Y, Zhang Q, Luo J, Jiang H *et al*. 2017. Phosphoprotein gene contributes to the enhanced apoptosis induced by wild-type rabies virus GD-SH-01 in vitro. Front Microbiol 8:1–13.

97. Upton JW, Shubina M, Balachandran S. 2017. RIPK3-driven cell death during virus infections. Immunol Rev 277:90–101.

98. Douzandegan Y, Tahamtan A, Gray Z, Nikoo HR, Tabarraei A, Moradi A. 2019.

Cell death mechanisms in esophageal squamous cell carcinoma induced by vesicular stomatitis virus matrix protein. Osong Public Heal Res Perspect 10:246–252.

99. Gadaleta P, Perfetti X, Mersich S, Coulombié F. 2005. Early activation of the mitochondrial apoptotic pathway in vesicular stomatitis virus-infected cells. Virus Res 109:65–69.

100. Wang Y, Kim NS, Haince JF, Kang HC, David KK *et al*. 2011. Poly(ADP-ribose) (PAR) binding to apoptosis-inducing factor is critical for PAR Polymerase-1-dependent cell death (Parthanatos). Sci Signal 4:ra20.

101. Sun L, Chen H, Ming X, Bo Z, Shin H-J *et al*. 2021. Porcine epidemic diarrhea virus infection induces caspase-8-mediated G3BP1 cleavage and subverts stress granules to promote viral replication. J Virol 95.

102. Takahashi M, Higuchi M, Matsuki H, Yoshita M, Ohsawa T *et al*. 2013. Stress granules inhibit apoptosis by reducing reactive oxygen species production. Mol Cell Biol 33:815–829.

103. Eisinger-Mathason TSK, Andrade J, Groehler AL, Clark DE, Muratore-Schroeder TL *et al*. 2008. Codependent functions of RSK2 and the apoptosis-promoting factor TIA-1 in stress granule assembly and cell survival. Mol Cell

31:722–736.

104. Iseni F, Garcin D, Nishio M, Kedersha N, Anderson P, Kolakofsky D. 2002. Sendai virus trailer RNA binds TIAR, a cellular protein involved in virus-induced apoptosis. EMBO J 21:5141–5150.